8-27-2009

Stimulated Brillouin scattering effects and suppression techniques in high power fiber amplifiers

Michael Zmuda

Follow this and additional works at: https://digitalrepository.unm.edu/ose_etds
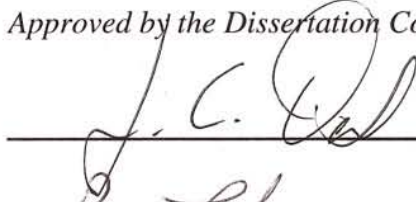
Michael Wayne Zmuda
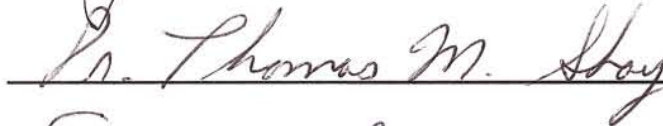*Candidate*

Physics and Astronomy
Department
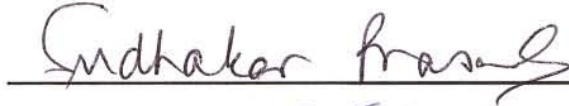
This dissertation is approved, and it is acceptable in quality
and form for publication on microfilm:
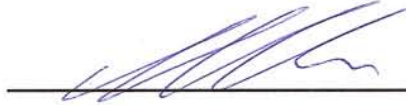
Approved by the Dissertation Committee:

_____, Chairperson

_____

_____

_____

_____

_____

_____

_____

STIMULATED BRILLOUIN SCATTERING EFFECTS AND

SUPPRESSION TECHNIQUES IN HIGH POWER FIBER AMPLIFIERS

BY

MICHAEL WAYNE ZMUDA
B.S., Physics, Cal Poly, 1987
M.A., National Security & Strategic Studies, Naval War College, 2006

DISSERTATION

Submitted in Partial Fulfillment of the
Requirements for the Degree of

Doctor of Philosophy
Optical Science and Engineering

The University of New Mexico
Albuquerque, New Mexico

August, 2009

DEDICATION

I dedicate this dissertation to my family, for without their encouragement, support, and faith in me I would never have been able to complete this journey.

To my brother Paul "Elijah" who encouraged me to learn and love math and science during my elementary school years. To my mom, always supportive and loving, who consistently told me that I could be whatever I desired. To my dad, who instilled a strong work ethic within me, continually and painfully challenged me to achieve excellence, and who defended me when others said I could not succeed. To my beautiful and loving wife who helped me through this Ph.D. journey during times of unemployment, military duty separation, cancer, severe diabetes, three promotions, and two wonderful children, Nathanael (34 months) and Naomi (14 months). To my brother in heaven who showed me how to be humble and serve others first. Above all, to my father in heaven who has always helped me and never abandoned me during the most significant challenges of my life.

ACKNOWLEDGMENTS

STIMULATED BRILLOUIN SCATTERING EFFECTS AND

SUPPRESSION TECHNIQUES IN HIGH POWER FIBER AMPLIFIERS

BY

MICHAEL WAYNE ZMUDA

ABSTRACT OF DISSERTATION

Submitted in Partial Fulfillment of the
Requirements for the Degree of

Doctor of Philosophy
Optical Science and Engineering

The University of New Mexico
Albuquerque, New Mexico

August, 2009

Stimulated Brillouin Scattering Effects and Suppression Techniques in High Power Fiber Amplifiers

by

Michael Wayne Zmuda

B.S., Physics, Cal Poly, 1987
M.A., National Security & Strategic Studies, Naval War College, 2006
Ph.D., Optical Science and Engineering, University of New Mexico, 2009

ABSTRACT

This dissertation develops a model for numerical analysis of stimulated Brillouin scattering (SBS) effects and the development of suppression techniques for the realization of increased output power levels for high power ytterbium-doped dual clad fiber amplifiers. The overall objective of this effort is to develop and validate a predictive model to assist in the determination of the most effective techniques for increasing SBS thresholds within ytterbium-doped fiber amplifiers in order to realize increased power output. The goal is to demonstrate an increase in SBS threshold that would increase the output power potential in ytterbium-doped fiber amplifiers by at least an order of magnitude. The approach determines the effect of changing the acoustic properties of fiber cores on the Brillouin frequencies and the effects of various signal modulation

schemes on active ytterbium-doped fiber amplifiers. In addition, temperature effects and temperature differentials within the fibers are predicted and measured, both with passive and active fibers. Brillouin center frequency responses of various germanium dopant concentrations within the cores, as well as the effects of fiber segment combinations are measured in the lab. The effects of various phase modulation schemes of the signal are predicted and measured for passive fibers. Results from these measurements are used to validate and adjust the model accordingly. Finally, the manufacturability of relevant characteristics required to achieve such SBS suppression is evaluated, identifying constraints and limitations for utilization of low cost fabrication techniques. The final model, validated and adjusted with empirical results, supports the suppression of SBS in standard ytterbium-doped fiber amplifiers by over a decade.

TABLE OF CONTENTS

LIST OF FIGURES

LIST OF TABLES

1   INTRODUCTION

1.1   MOTIVATION

The desire to develop high power lasers has been a goal by both private industry and the United States military for over three decades. Although the first high power lasers were based on chemical laser concepts, solid state and fiber lasers have many advantages and potential benefits over chemical lasers; advantages that include size, weight, and preferable pumping mechanisms. High power (>100kW) applications requiring transmission through the atmosphere at long distances (>3km), however, require exceptional beam quality (M^2<1.5). The most promising high power fiber laser approaches to achieve these high powers with exceptional beam quality are based on coherent beam combining (CBC) of multiple fiber amplifiers. Due to the nature of CBC, each fiber must be single mode with a very narrow linewidth (<100MHz). In addition, the number of fibers to be combined is finite, so that each fiber must reach high power with a very narrow linewidth. There are several barriers, however, that must be overcome before such benefits can be realized; such barriers include nonlinear effects that limit single fiber amplifier and laser output power. Stimulated Brillouin scattering (SBS) is the dominant nonlinear effect that limits such single fiber high power outputs. Overcoming SBS limits on a single, narrow linewidth, fiber amplifier output power will provide the ability to achieve the >100kW power levels through CBC approaches.

1.2   OVERVIEW

Advanced laser concepts utilizing fiber amplifiers and fiber lasers are limited in power output by SBS thresholds. A high intensity laser source can create an acoustic wave in the fiber through the process of electrostriction[1]. This acoustic wave will then

create refractive index variations within the fiber which in-turn scatter the source light through Bragg diffraction[2]. The scattered light will be Doppler downshifted in frequency by the index grating which is moving at the acoustic velocity. The scattered, or Stokes, wave will beat with the incident pump giving rise to additional acoustic waves.
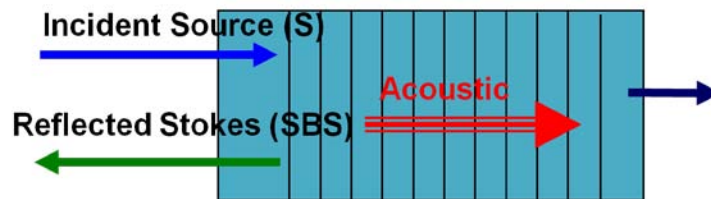
Figure 1: SBS in single mode fibers

This non-linear self-feeding mechanism is limited by the incident source power.

As the incident source power is increased, it will reach a threshold in which additional output power will be converted into the backward scattered Stokes wave. We define the SBS threshold as the point where the Stokes power reaches 1.0% of the incident power. As the incident power increases, the first order Stokes power increases rapidly until a second order Stokes wave in the opposite direction causes the first order Stokes power to reach threshold. The output power of the fiber will then begin to increase because of the addition of the second order Stokes wave to the transmitted source power. Thus, increasing the incident source power will continue to increase both the forward and backward signals as multiple Stokes waves in both directions reach threshold. The problem, however, is that there will be multiple output frequencies, downshifted both multiples of two of a signal downshifted Stokes wave.
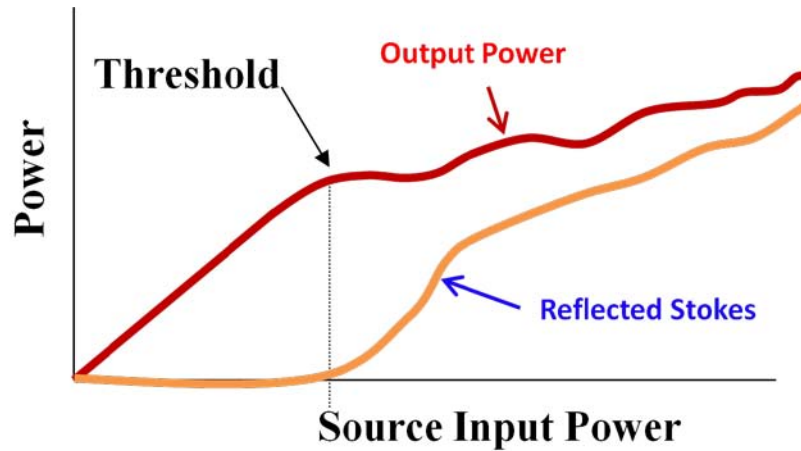
Figure 2: SBS power threshold

It has been shown that SBS threshold depends on several factors, including the spectral width of the pump wave, the length of the fiber, temperature, and fiber core diameter [1-24]. Changing the germanium dopant concentration of single mode fibers and cascading them together has demonstrated the ability to decrease the SBS threshold[25]. Phase modulation of the pump signal has been shown to decrease SBS threshold as well as the effective SBS gain by changing the phase of the pump wave E-field, thus increasing the effective pump wave spectral width [26-28].

Figure 3 shows a brief history of published fiber laser and amplifier systems over the past several years through January, 2007. It demonstrates the remarkable improvement in the output power of a single mode beam. The red line represents commercial single mode, large linewidth, product development while the blue, green, and dashed orange lines indicate progress in laboratory demonstrations.
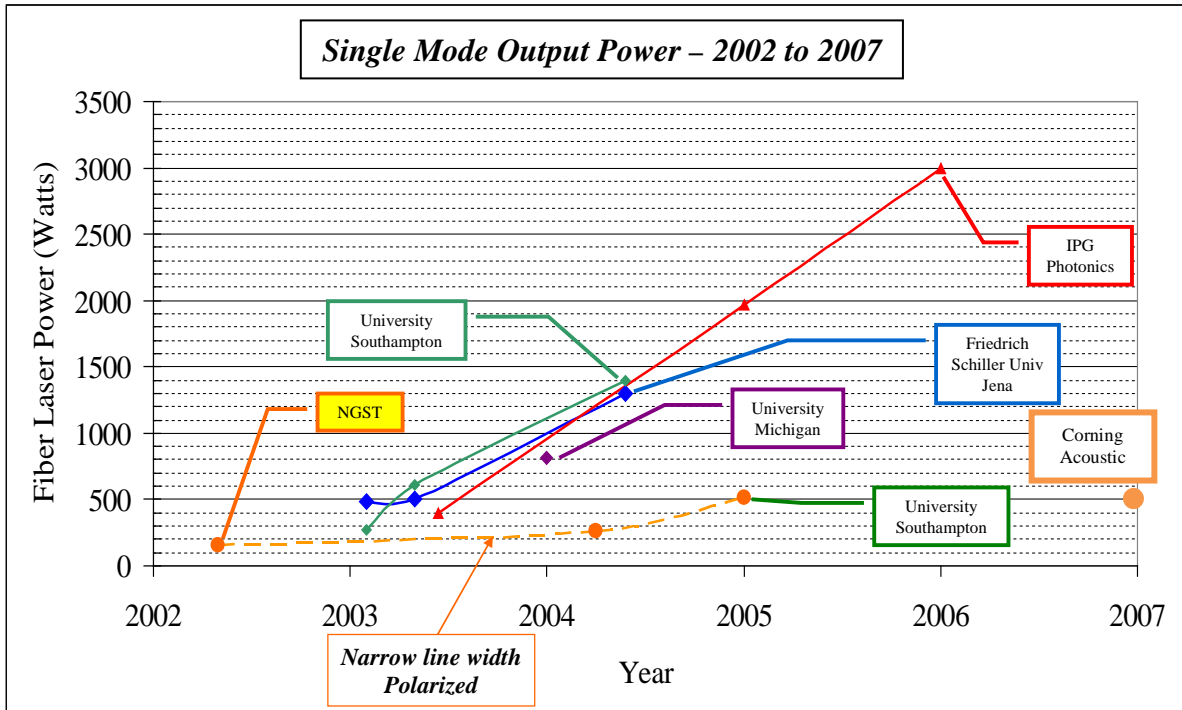
Figure 3: History of fiber laser developments

The highest reported power from a very narrow linewidth fiber amplifier (<150 MHz) is approximately 500 W [29]. The fiber used was an Yb-doped conventional large mode area (LMA) double clad fiber. LMA fibers are, however, generally limited in practice to less than 30 μm in core diameter for single mode operation[30]. Furthermore, due to the low numerical aperture (NA) of these fibers, it is difficult to achieve high Yb-dopant levels that can lead to a reduction in fiber length as Yb is an index-increasing dopant.

Methods such as the introduction of a thermal gradient in an end-pumped optical fiber have been implemented and were successful in increasing the power available from narrow linewidth fiber amplifiers from less than 100 W to the current 500 W [5]. In 2007, an acoustic mode suppressive design fiber has been pushed by Corning to the high power

4

regime (~500 W) [31, 32]. The Corning method is based on the reduction of the overlap between the optical and acoustic modes supported by the waveguide. Additional experimental demonstrations of acoustic mode suppressive designs have since been performed without significant increase in power output[32-35]. Finally, Nilsson et al., reported at the 2009 Photonics West conference in San Jose, California, that their team recently achieved over 1.5 kW for a single fiber through an unknown (not cleared for public release) method or combination of techniques[36]. The linewidth, however, was >300 MHz with an M^2 > 1.6-not suitable for current coherent beam combining desired for high power applications (>100 kW).

Recent commercial developments include 410 W, single frequency, and high beam quality for a fiber amplifier made by IPG Photonics, as well as a 6.0 kW single mode, large linewidth (~THz), with low M^2 beam quality (<1.1)[37]. Corning also recently achieved near 1.0 kW large linewidth with their SBS suppressive fiber[38]. Many of these output power improvements were made possible with the use of large fiber core diameters[38]. Low numerical apertures and other concepts such as bend loss were used to maintain high beam quality in the laser output. Unfortunately, it becomes increasingly difficult to maintain high beam quality as the core size grows, as demonstrated by the M^2 value of ~4.0 for the aforementioned Corning fiber. In addition, bending decreases the mode area as a result of the deformation of the mode field distribution[38, 39].

Although it would be convenient to bundle multiple fibers together to achieve the required power of tens of kilowatts, power is not the only measure of how useful a laser system can be. If it were, then beam quality would not be a factor limiting the core size

of our fiber laser systems. Brightness is a more robust measurement that incorporates not only the power, but also the beam quality. For this reason, SBS mitigation techniques must incorporate the ability to ensure fiber power scaling through coherent beam combination, not just single fiber output power.

The goal of this dissertation is to develop and validate a predictive model to assist in the identification of the most promising techniques for increasing SBS thresholds within ytterbium-doped fiber amplifiers in order to realize increased power output by at least an order of magnitude. The approach is to determine the effect of Ge-dopant concentrations on Brillouin frequencies and the effects of various signal modulation techniques on active ytterbium-doped fiber amplifiers. Brillouin frequencies of various Ge-dopant concentrations as well the effects of fiber segment combinations will be measured in the lab. In addition, the effects of various modulated signals and modulation schemes will be measured. Results from these measurements will be used to develop validated models.   Results from these models will be used to determine the most effective way to combine fibers of differing Ge-dopant concentrations and with various signal modulation schemes. Model predictions will be validated empirically.

1.3   UNIQUENESS OF RESEARCH

This research develops a model utilizing standard fiber manufacturing techniques currently available, along with inherent characteristics of fiber amplifiers, and current approaches to beam combining to realize a cost effective, repeatable solution. Specifically, this research: 1) develops a design model utilizing current low-cost manufacturing capabilities; 2) acquires accurate SBS responses utilizing a novel approach for measuring temperature, core density, and phase modulation variations, including

linewidths, line shapes, and peak frequency; 3) acquires first ever direct measurement of SBS line shape in a thermal gradient for active ytterbium-doped dual clad fibers; 4) includes a truly iterative model development through sequentially more complex experimental configurations and results; 5) develops first ever design of cascading Dual Clad Fibers for increasing SBS threshold; 6) develops first ever thermal model for double clad fiber structure; and 7) identifies technique for adjusting thermal gradient along fiber to minimize SBS.

1.4   DOCUMENT ORGANIZATION

This dissertation is organized in the same order as the model development. Initially, the background and theory is presented in a manner to support initial model development. Based on this information, initial assumptions, limitations, and approaches are identified and used for the model. Specifically, the effects of phase modulation, density differentials, and temperature effects are developed. Next, passive fiber selection, rationale, and constraints, followed by the experimental set-up and results are presented. Experiments are utilized to determine effects of Stokes center frequency shift, linewidth, and shape as a result of temperature, density, and phase modulation of input signal. Information from these results is then utilized to adjust or validate the model. The selection, constraints, and specifications for the active dual cladding ytterbium doped fiber amplifiers are then presented. Phase modulation is not included in this portion of the development. Experimental set-ups for evaluating thermal gradients and density variations are presented followed by the associated results. Based on these results, final theoretical model adjustments are made in order to predict the combination of techniques and manufacturing capabilities required to increase SBS threshold by over a decade for a

single dual clad fiber amplifier utilizing standard manufacturing techniques. A summary of the results with recommendations and limitations for future research and made in the final chapter.

2 THEORY, ASSUMPTIONS, AND MODEL DEVELOPMENT

2.1 FIBER AMPLIFIERS

In order to understand and model the effects of SBS within fiber amplifiers, a basic understanding of the fiber amplifier must be reached. Fiber amplifiers utilize rare earth ions within optical glass fibers as a gain medium. Such rare earth ions include erbium, neodymium, praseodymium, thulium, and ytterbium. Optical fibers were first used and demonstrated in the early 1960s to reduce the required pump power for gain in glass amplifiers by Snitzer [7]. It wasn't until the 1980s, however, until the optical communications industry demand generated a greater need for fiber amplifier applications. With the growing capacity of higher power pump diodes, the incentives of the communications industry, and supportability and fabrication technologies associated with silica based fiber, methods for fabricating rare earth doped silica-based fibers have continued to develop [8].

Operation of these fiber amplifiers is relatively simple. The active dopant - rare earth ion - is pumped utilizing high power laser diodes. The pump light propagates through the fiber, continually pumping the rare earth ions through the length of the fiber. A second laser source at a larger wavelength will be amplified through stimulated emission as it propagates the length of the fiber. As a result of the relatively long length of the fiber, almost all the pump source can be absorbed, providing a high gain to the signal. The figure below is a depiction of a simple erbium doped fiber amplifier, including two pigtailed optical isolators to mitigate damage from reflections, as well as being both co-pumped and counter-pumped:
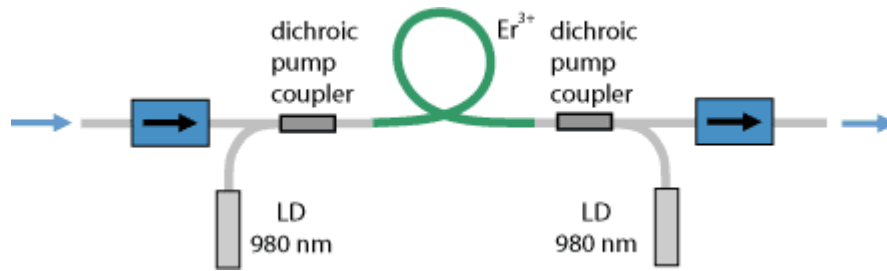
Figure 4: Erbium doped fiber amplifier, pumped at 980 nm and operating at 1064 nm [40]

Although initial pumping schemes co-utilized the fiber core for pumping, more recent designs include a double clad structure to increase pump power insertion. In this design, the signal propagates through a single mode core while the pump propagates through a larger multimode pump guide, as well as the core, surrounded by a second clad. The core contains the active medium. The pump is launched into the cladding at either or both of the fiber ends and propagates in a "zig-zag" pattern through the doped core. The first clad utilizes a large numerical aperture of ~0.46 to provide a broad acceptance angle to couple the lower brightness pump laser diode source. In order to relax this high numerical aperture value, higher brightness laser diodes will need to be developed. Typically, the core has a much smaller numerical aperture to maintain single mode operation, ~0.06 – 0.16. The ratio of the clad to core diameter is proportional to the amount of pump introduced into the core. By reducing this ratio while increasing rare earth dopant concentrations, shorter fiber amplifier lengths will be permitted. The following is a depiction of a dual clad configuration and operation:
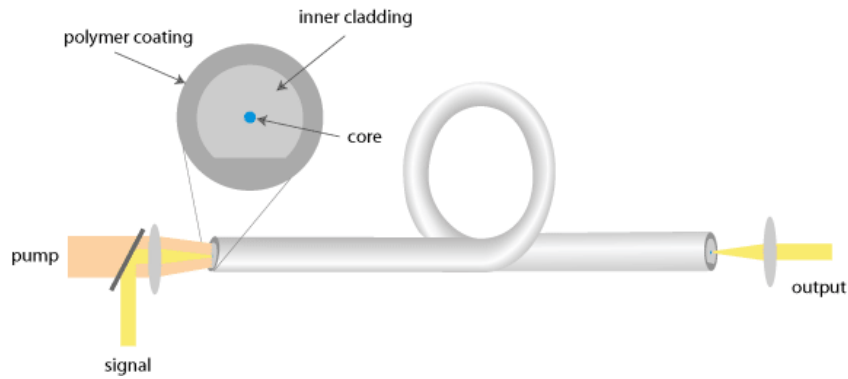
Figure 5: Dual clad fiber example using D-clad configuration [40]

To avoid skew angle propagation of the pump, thus missing the core, various first cladding configurations have been used, including the following:

Figure 6: Dual clad configurations [40]

Nufern has created their version of a dual clad fiber amplifier configuration utilizing an octagonal cladding architecture, surrounded by a second cladding material with excellent thermal insulating properties. There are still other dual clad designs being developed, including photonic crystal fibers (PCF). PCF use air holes within the cladding to permit greater numerical aperture values and aide in keeping pump light away from the protective polymer coating on the surface.

For higher gain fiber amplifiers, resulting in higher power signal output, the rare earth dopant must be increased. There are limits, however, on the ability of increasing such concentrations. In order to increase the solubility of the rare earth ions, other dopants are added to the glass host composition [41]. When the host glass composition

11

utilizes such elements as germanium or phosphorus to raise the index of the core, aluminum oxide is typically used to increase the rare earth ion solubility [41]. These additions, however, are limited due to the effects on fluorescence lifetime, absorption, emission, and excited state absorption cross sections of the dopant transitions [41]. For this reason, typical rare earth concentrations are currently limited to about 2% [41].

For many of the rare earth ions used in fiber amplifiers, an effective three level energy transition scheme is used. Standard rate equations using absorption and emission cross sections can be used to determine effective power gains for the propagating signal. ytterbium, however, can be reduced to a simplified two energy level transition.

There are also nonradiative transitions for all rare earth ions. Nonradiative transitions result in an increase of temperature within the fiber core. However, because of the thermal conductivity of the glass, heat escapes the fiber without significant increase in temperature for lower pump power operation. For higher pump powers, the thermal differential along the fiber length could be hundreds of degrees.

2.2   SPECIAL PROPERTIES OF YTTERBIUM-DOPED GAIN MEDIA

Ytterbium is perhaps the best suited rare earth ion for fiber amplifiers for many reasons. First and foremost, ytterbium has an extraordinarily wide absorption and fluorescence bands [41-43]. Figure 7 shows this wide range through the cross sections of both absorption and emission:
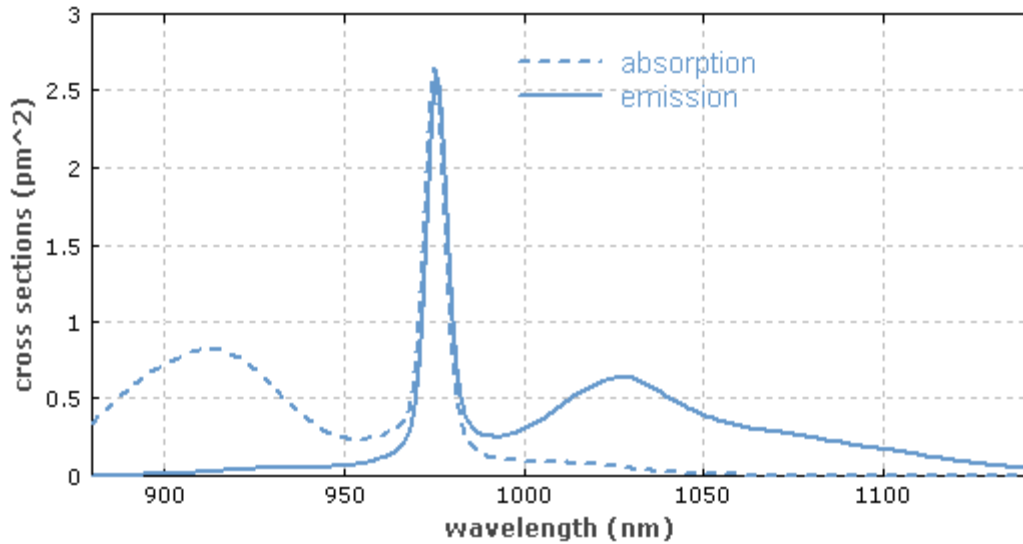
Figure 7: Effective absorption and emission cross sections of Yb^{3+}-doped germanosilicate glass [40]

The wide range in absorption wavelengths, from ~850 nm to 1070 nm, permits Yb-doped fiber amplifiers to be pumped with several types of lasers and laser diodes, as well as permitting various pumping schemes. Also, the wide range of amplification, ~970 nm to 1200 nm, permits wavelength tuning to support many unique applications or the pumping of other lasers operating in the "eye-safe" region of 2.0-5.0 um. In addition, the extremely high absorption and emission cross sections permit high output power and excellent power conversion efficiency [44]. These are typically higher than other rare earth ions, thus permitting strong pump absorption resulting in shorter fiber amplifier lengths [41].

Now, the energy level diagram for Yb^{3+} is extremely simple, having only two relevant states-a ground state manifold (^{2}F$_{7/2}$) and only one excited state, a metastable state manifold (^{2}F$_{5/2}$). Other levels are outside our concern within the ultraviolent regime

[41]. Pumping and amplification occur between the four ground state sublevels, i-l, and three excited state sublevels, a-c, as depicted below:
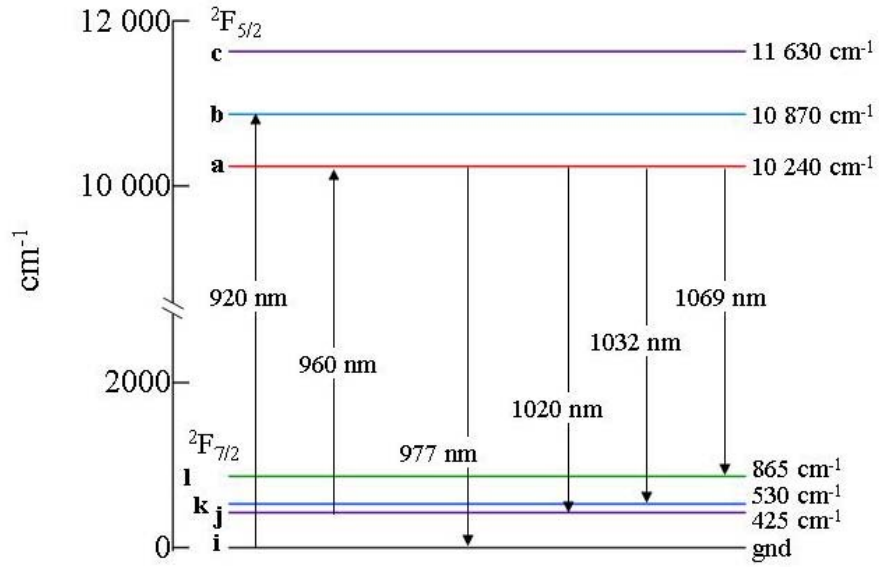
Figure 8: Energy level diagram of Yb^{3+} in silica[43]

Also, the upper-state lifetimes are relatively long-typically ~1.0-2.0 ms, the quantum defect small, and an electronic structure that excludes excited state absorption, all contributing to high power efficiencies [42]. Finally, slope efficiencies or Yb-doped dual clad fibers have been reported as high as 75% by Nufern, compared with 40% for Er-Yb doped amplifiers.

For the fiber amplifier system used for this dissertation, the pump transition, 977 nm, is from the "i" sublevel in the $^2F_{7/2}$ manifold to the excited "a" sublevel within the $^2F_{5/2}$ manifold, while the lasing, 1064 nm, transition is from the "a" sublevel within the $^2F_{5/2}$ manifold to the "l" sublevel in the ground $^2F_{7/2}$ manifold state. The quantum

efficiency is related to the difference in energy between the pump and emission, given by:

$$\eta = \frac{\lambda_{laser} - \lambda_{pump}}{\lambda_{laser}}.$$

(1)

The quantum efficiency for this dissertation arrangement, as a result of using the peak absorption of 976 nm coupled with the standard 1064 nm wavelength for lasing, is 0.083. This value is related to the nonradiative transitions resulting in the generation of heat within the core.

2.3   COHERENT BEAM COMBINING

Achieving effective power scaling for power levels in the tens of kilowatts requires independent beam combining. Although wavelength beam combining (WBC) is another technique, we shall focus on coherent beam combining (CBC) due to current research focus within the high power laser community. Temporally incoherent beams (N) with brightness "B_1" and power "P" for each beam combine to provide a total brightness "B" as [45-47]:

$$B = \frac{NP}{\Omega(NA)} = B_1,$$

(2)

while coherent beams (N) of brightness B_1 combine as:

$$B = \frac{NP}{(\Omega/N)(NA)} = NB_1.$$

(3)

For CBC, the illustration in Figure 9 depicts the two conditions stated above.
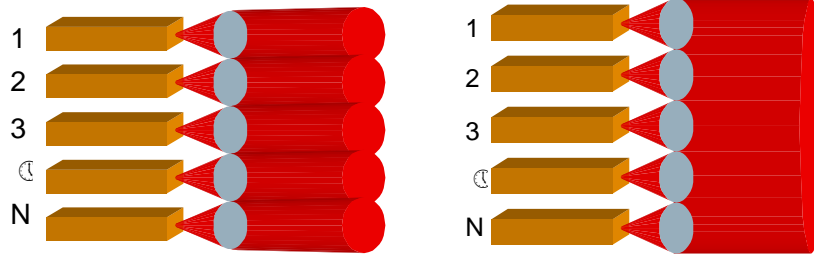
Figure 9: Non-coherent versus coherent beam combining

From this, for coherent beams, we can power scale by the factor "N". In addition, the brightness of each fiber beam is dependent upon the beam quality (M^2) according to the definition of brightness given by Fan[46]:

$$B_1 = \frac{CP}{\lambda^2 (M^2)^2},$$

(4)

where C = 1 for TEM00 gaussian beams.

Although fiber amplifiers have been reported to achieve near the kilowatt power, they are done so with large M^2 values, thus minimizing their ability to be power scaled through CBC. For low M^2, a master oscillator power amplifier array approach can simplify the coherent combination process [46, 48]. If each element of the amplifier array were absolutely identical, no compensation would be required to maintain perfect phasing of each element. Unfortunately, the amplifiers will have slightly different lengths, have small fluctuations in temperature, be pumped at different powers, and have a myriad of other non-uniformities that destroy the phase front at the end of the fiber[49].

The amount of acceptable variation between elements is strongly dependent on the master oscillator bandwidth—the greater the bandwidth, the shorter the coherence length and therefore the tighter the tolerances [50]. This alone encourages one to use very narrow linewidth sources. The undesired side effect, however, is a reduction in SBS

threshold. Typical high power systems being developed today have broad spectral bandwidths to help mitigate SBS, but this also reduces their overall effectiveness for coherent combination. The goal, therefore, should be to increase SBS threshold, while maintaining narrow bandwidth operation ~100 MHz with $M^2 < 1.5$.

2.4 SBS POWER THRESHOLD

The following estimation for SBS power threshold in fibers was introduced by Smith in 1972 and modified by others to improve its accuracy[19]:

$$P_{th} = C \frac{kA_{eff}}{g_B L_{eff}} \left(1 + \frac{\Delta \nu_s}{\Delta \nu_p} \right).$$

(5)

Here "C" is a constant, typically assigned a value of "21" for fibers, "k" is a factor relating to the effects of polarization (1<k<2), "g_B" is the SBS gain coefficient discussed in section 2.8, "A_{eff}" is the mode field area within the core, and "L_{eff}" is the effective length of the fiber. Although the trends related to this equation remain consistent, the value of the constant "C" changes depending on the conditions under which the fiber amplifiers operate. From this relationship, it is apparent that larger fiber cores will result in a higher power threshold, while longer lengths result in a lowered power threshold. By increasing the effective area and the probe bandwidth while maintaining short effective lengths, the threshold can be kept very high.

Although this threshold relationship is for passive fibers, the general conclusions regarding SBS threshold hold true for fiber amplifiers. Due to the increasing power of

the pump near the end of the fiber, the effective length will change accordingly. In addition, the effectives of temperature differentials along the fiber length due to the heat dissipated from nonradiative processes will also change the effective length. These special considerations will be discussed further and utilized in the development of our model.

2.5   SBS MITIGATION TECHNIQUES BY OTHERS

As shown in section 2.4, the SBS threshold is proportional to the field diameters of the mode in the fiber--A_{eff}. Increasing A_{eff} would therefore increase the threshold power. This was the first and simplest mitigation technique used by many within the fiber amplifier community.

If the power carried by the fiber is spread out over a larger area, intensity decreases as does the possibility for non-linear interaction. If beam quality is not an issue, the core size of a fiber can be made large enough to support a fiber amplifier capable of 50 kW[51]. This type of industrial laser is commercially available today. IPG currently provides a variety of industrial and government organizations such lasers on board a variety of platforms for specialized uses. These applications are limited to shorter distances due to the poor beam quality and associated beam spread.

However, if one is concerned with beam quality, as discussed previously, a much more stringent parameter is placed on the fiber. One must attempt to scale core size while maintaining single transverse mode operation. Currently the largest truly single mode, step-index fiber has a mode field diameter of approximately 10-12μm. An amplifier, without additional SBS mitigation techniques, with this core size will, at best be capable of ~100W. Fortunately there are a few tricks that allow for larger core fibers

to be used. Specifically, waveguide modes are subject to losses if the fiber is bent or coiled. Higher order modes see a greater loss than the fundamental mode in a regular step index fiber. A large mode area (LMA) fiber, which when un-bent may support ten (10) transverse modes, can be coiled to filter higher order modes leaving only the fundamental.

Other techniques recently used to mitigate SBS include extremely expensive specially manufactured fibers or unique launch conditions. Many include varying radial densities or longitudinal stresses to change the response of the acoustic velocity within the fiber region core [11, 33, 52-54]. One recent approach includes the use of two "seed" signals of slightly different frequencies, named "two-tone", where each of the "tones" reach SBS threshold independently[55, 56]. PCFs are rapidly becoming a primary focus for high power fiber laser research. These fibers guide light through a periodic array of microscopic air holes along the length of the fiber. Such designs permit larger effective core diameters while maintaining single mode propagation, as well as permitting improved pump area[54, 57]. Although these techniques have proven success on an individual scale, budget constrained environments require the use of more readily available—and cheaper—commercial-off-the-shelf components and associated launch and pumping schemes.

Larger core diameters with stringent launch conditions and expensive specialty fibers-acoustic, PCF, and other designs-may incur costs associated with peripheral pumps and set-ups that exceed current budget limitations for mass applications. As a result, such approaches, although novel and useful, may not have the ability to be deployed-especially for the longer ranges and higher powers required for strategic targets. For this reason, a

more thoughtful approach using current capabilities, manufacturability, and within a robust adverse environment must be considered.

2.6   ACOUSTIC VELOCITY

In examining techniques to mitigate SBS in fiber amplifiers, one must further understand the nature and characteristic of SBS in fibers. Conservation of energy and phase requires[2]:

$$\Omega_B = \omega_p - \omega_s,$$
$$k_A = k_p - k_s,$$

(6)

where Ω_B, ω_P, and ω_s, are the Brillouin, pump, and Stokes frequencies, respectively, while k_A, k_P, and k_S are the acoustic, pump, and Stokes wave vectors, respectively.

The Brillouin frequency can be related to the acoustic wave vector through the dispersion relation[2]:

$$\Omega_B = v_A \left| k_A \right| \approx 2 v_A \left| k_p \right| \sin\left(\frac{\theta}{2}\right),$$

(7)

where v_A is the acoustic velocity within the medium.

If we limit our fiber applications to single mode where only forward and backward directions exist, Equation 3 reduces to[2]:

20

$$v_B = \frac{\Omega_B}{2\pi} = \frac{2nv_A}{\lambda_p};$$

$$\text{where } |k_p| = \frac{2\pi n}{\lambda_p}.$$

(8)

From this we see that the acoustic velocity within the fiber core can play a significant role in determining how we might mitigate SBS. By changing the properties of the acoustic velocity within the fiber, one would change the corresponding SBS effect. If the center Brillouin frequency was shifted beyond its width, then the effect of SBS threshold would be mitigated.

2.7   PARAMETERS AFFECTING ACOUSTIC VELOCITY

To mitigate the effects of SBS, we need to determine the relationship by which physical parameters affect the acoustic velocity in fibers. The equation of motion for a pressure wave stated by Boyd as given by Fabelinskii, 1968 [1, 58]:

$$\frac{\partial^2 \Delta\tilde{p}}{\partial t^2} - \Gamma'\nabla^2 \frac{\partial\Delta\tilde{p}}{\partial t} - v_A^2\nabla^2\Delta\tilde{p} = 0,$$

(9)

where p=Pressure, t=Time, ρ=Density, and v_A =Accoustic Velocity.

The acoustic velocity from a pressure wave can be written in terms of thermodynamic variables as follows [1]:

$$v_A^2 = \left(\frac{\partial p}{\partial \rho}\right)_s.$$

(10)

Compressibility is defined as the following [1]:

$$C \equiv \frac{1}{K} = -\frac{1}{V}\frac{\partial V}{\partial p} = \frac{1}{\rho}\frac{\partial \rho}{\partial p}, \qquad (11)$$

where:

C=Compressibility, K=Bulk Modulus, and V=Volume.

For solids and liquids involved in non-diffusive, adiabatic processes [7]:

$$\frac{dT}{T} = -\left(\frac{\beta}{C_T c_V}\right)dV = \left(\frac{V\beta}{c_P}\right)dp, \qquad (12)$$

where:

T=Temperature, β=Coefficient of Thermal Expansion

C_T =Isothermal Compressibility; and c_V ,c_p =Heat Capacities.

We will assume an adiabatic process occurs. This leads to:

$$\Rightarrow -\frac{1}{V}\frac{dV}{dp} = C_T \frac{c_V}{c_p}. \qquad (13)$$

At room temperature or above, the heat capacities at constant temperature and constant volume are nearly equal [59]. Both the Debye and Einstein models give heat capacity = $3N_a k$ for temperatures greater than room temperature.

Debye Model:

$$E = 9N_a \frac{(kT)^4}{\varepsilon_{max}^3} \int_0^{\varepsilon_{max}/kT} \frac{x^3}{e^x - 1}dx \cong 3N_a kT \text{ @ high temp} \qquad (14)$$

Einstein Model:

$$E = 3N_a \frac{\hbar\omega_0}{e^{\frac{\hbar\omega_0}{kT}} - 1} \cong 3N_a kT \text{ @ high temp} \tag{15}$$

Heat Capacity:

$$\frac{dE}{dT} = 3N_a k \text{ @ high temp(300K+)} \tag{16}$$

Compressibility can be measured either at constant temperature or at constant entropy and are related as follows [1]:

$$\frac{C_T}{C_S} = \frac{c_p}{c_v} \Rightarrow C_S = C_T \frac{c_v}{c_p} \cong C_T. \tag{17}$$

From equations 12, 13 and 17 we obtain the following:

$$C_S = \frac{1}{\rho}\left(\frac{\partial\rho}{\partial p}\right)_S = \frac{1}{\rho v_A^2} \cong C_T, \tag{18}$$

$$\Rightarrow v_A = \sqrt{\frac{1}{C_T\rho}} = \sqrt{\frac{K_T}{\rho}}. \tag{19}$$

The acoustic velocity in a fiber core is equal to the square root of the Bulk Modulus divided by the density. If we assume the densities of our fiber cores do not change within our operating temperature range, then the temperature dependence for the velocity of sound is the temperature dependence of the bulk modulus. Temperature dependence of the bulk modulus must be determined empirically.

$$\Rightarrow v_A = \sqrt{\frac{f(T)}{\rho}};$$

where $f(T)$ increases with temperature.

(20)

To obtain the $f(T)$ in a fiber, one could conduct an SBS experiment with varying temperatures. From this, the effects and relationships of temperature and densities would be known for the acoustic velocity, and, in turn, the associated effects on SBS. Temperature dependence experiments have been conducted for passive fibers and are presented in Chapter 5.

2.8   SBS COUPLED EQUATIONS AND GAIN SPECTRUM

The development of the non-linear coupled equations and associated gain spectrum for SBS has been completed for passive fibers by Boyd and others [1, 19, 60]. Under steady state conditions, time derivatives vanish such that the non-linear coupling among the three interacting waves-the pump, the Stokes, and the acoustic waves-are reduced to two coupled non-linear equations. Setting the two frequencies equal, due to the small shift from the acoustic velocity, and assuming that the fiber loses are the same for both the pump and Stokes waves, the coupled steady-state intensity equations become[1, 2]:

$$\frac{dI_P}{dz} = -g_B I_P I_S - \alpha I_P,$$

$$\frac{dI_S}{dz} = -g_B I_P I_S + \alpha I_S,$$

(21)

where I_P, I_S, g_B, and α, are the pump intensity, Stokes intensity, Brillouin gain coefficient, and fiber loses, respectively. The Brillouin gain coefficient or "gain factor" has a

Lorentzian spectrum, related to the acoustic damping time or phonon lifetimes, and is given by[1]:

$$g_B = g_0 \frac{\left(\Delta \nu_B / 2\right)^2}{\left(\nu - \nu_B\right)^2 + \left(\Delta \nu_B / 2\right)^2} = g_0 \frac{1}{1 + \left[2\left(\nu - \nu_B\right)/\Delta \nu_B\right]^2}. \quad (22)$$

"g_0" is the peak value occurring when ν is at ν_B, given by[61, 62]:

$$g_0 \equiv g_B\left(\nu_B\right) = \frac{2\pi n_{core}^7 p_{12}^2}{c\lambda^2 \rho_0 \nu_A \Delta \nu_B}, \quad (23)$$

where p_{12}, Γ_B, λ, and ρ_0 are the longitudinal elasto-optic coefficient, Brillouin linewidth, wavelength of the source, and core density respectively. The full width at half maximum (FWHM) of the gain spectrum, $\Delta \nu_B = \Gamma_B/2\pi$, is inversely proportional to the phonon lifetime within the core, $T_B = \Gamma_B^{-1}$, where T_B is the phonon lifetime[2]. Actual values of g_0 for optical fibers change according to the material properties and manufacturing processes, however, the value of 5 x 10^{-11} m/W is typically used[2].

The Stokes wave is initiated from thermally excited acoustic waves - spontaneously generated phonons - at the opposite end of the fiber from the signal entrance [19, 60]. Typical stokes wave power values used for initiation of Stokes are between 10^{-11} and 10^{-12} of the signal power. These values have been compared with statistical estimates from Smith and are in agreement. An estimate for the initiation of noise at the end of the fiber can be derived from Grower, giving the following [63]:

$$I_{SBS}\left(L_{fiber}\right) = \frac{kTc\Delta \nu_{SBS}}{\lambda_{SBS} \nu_{SBS} A_{core}}, \quad (24)$$

where A_{core} represents the area of the core, L_{fiber} represents the end of the fiber opposite of the signal (what we have called the pump for a passive system), and λ_{SBS} represents the wavelength of the Stokes (this value and the signal are so close that we will use the signal for our model).

Now, the rate equations above are for passive fibers, and therefore do not account for the amplification and pumping schemes required for our model. Before we continue, a brief discussion of the appropriate pumping scheme is needed to identify the most effective model.

From the rate equations in section 2.9, we see that the change in the Stokes intensity is proportional to the signal intensity. The pump power falls off exponentially as it propagates along the fiber length, thereby delivering exponentially less "pump" to excite the ytterbium ions within the core along the length of the fiber. Since the gain is proportional to the number of excited states, the gain will also diminish exponentially. If we pump from the signal entrance end of the fiber, we will have the majority of our gain near the entrance, thus creating a long propagation distance for a higher power signal. On the other hand, if we counter-pump, we will have the majority of the initial fiber length with lower signal power and only create a high power signal for a shorter distance near the end of the fiber. Since SBS threshold is dependent on the signal power and effective length, a counter-pumping scheme will significantly reduce SBS. For this reason, we shall use a counter-pumping scheme for our model.

In a fiber amplifier, we must include gain for both the propagating stokes and the signal waves within the core. In addition, we must account for the "pump" source which is depleting as it "pumps" the ytterbium within the core. Since the use of the term

"pump" is now duplicative, we will provide a new nomenclature to avoid any confusion. From now on, the initial signal will be labeled with a subscripted "s", the Stokes or Brillouin related items will be labeled with a subscripted "SBS", and the forward and backward "pump" will be labeled with a subscripts "f" and "b", respectively. The subscript "p" represents generically the pump for either forward or backward directions. "Γ" with the appropriate subscripts represents the overlap factor (not to be confused with the Brillouin linewidth designated with a subscript "B") between the light-field modes and the ytterbium distribution. The use of "I" for intensity will be replaced with a "P" for power. To adjust for the extra dimension of area in the conversion, the P_{SBS} will be divided by "A_{eff}" – equivalent to the area of the mode field diameter (MFD) of the core. The use of the symbol "σ" will be used for cross sections with the superscript of "e" and "a" representing emission and absorption, respectively. Utilizing the simplified energy level interaction of ytterbium, N_2 and N_1 reflect the ion population density in the upper and lower levels. Neglecting intrinsic background loses, due to the overwhelming large gain due to amplification by comparison, we have the following rate equations for a counter-pumped ytterbium dual clad fiber amplifier, modified from Liu[18]:

$$\frac{dP_s}{dz} = (N_2\sigma_s^e - N_1\sigma_s^a)\Gamma_s P_s - P_s g_{SBS} P_{SBS} / A_{eff}, \tag{25}$$

$$\frac{dP_f}{dz} = (N_2\sigma_p^e - N_1\sigma_p^a)\Gamma_p P_f - P_f g_{SBS} P_{SBS\_Clad1} / A_{Clad1}, \tag{26}$$

$$\frac{dP_b}{dz} = -(N_2\sigma_p^e - N_1\sigma_p^a)\Gamma_p P_b - P_b g_{SBS} P_{SBS\_Clad1} / A_{Clad1}, \tag{27}$$

$$\frac{dP_{SBS}}{dz} = -(N_2\sigma_s^e - N_1\sigma_s^a)\Gamma_{SBS} P_{SBS} - P_s g_{SBS} P_{SBS} / A_{eff}. \tag{28}$$

The second terms for the change of the forward and backward pump equations accounts for any SBS within the first cladding resulting from the pump power. The area of the clad is very close to the mode field area so the physical dimensions of the clad are used. Since our model will ensure that the threshold for the signal will not be exceeded with our pump a power level that is within an order of magnitude of the signal and a clad area several orders of magnitude greater than that of the core, these two terms can be neglected. These coupled rate equations now account for the dominant terms and interactions related to a co- and counter-pumped fiber amplifier. For either a co- or counter-pump only scheme, the opposite pump equation can be removed.

The overlap factors for dual clad fiber amplifiers can be approximated for use in our model. Since the signal and Stokes frequency are nearly identical, separated by ~16 GHz, we will assume that the associated overlap factors are nearly the same. Since we are given the mode field diameters (MFD) for our fibers, we will use this value as a reference. The MFD represents the width of the Gaussian beam at $1/e^2$ power, or 0.135 times the maximum value. Also, the overlap of the pump will be the ratio between the areas of the core to that of the first cladding. For the areas, "d_{core}" and "$d_{cladding}$" represent the diameter of the core and cladding, respectively. Our final coupled rate equations are as follows:

$$\frac{dP_s}{dz} = (N_2\sigma_s^e - N_1\sigma_s^a)\Gamma_s P_s - P_s g_{SBS}P_{SBS} / A_{eff},$$ (29)

$$\frac{dP_f}{dz} = (N_2\sigma_p^e - N_1\sigma_p^a)P_f \left(\frac{d_{core}}{d_{cladding}}\right)^2,$$ (30)

$$\frac{dP_b}{dz} = -(N_2\sigma_p^e - N_1\sigma_p^a)P_b\left(\frac{d_{core}}{d_{cladding}}\right)^2, \tag{31}$$

$$\frac{dP_{SBS}}{dz} = -(N_2\sigma_s^e - N_1\sigma_s^a)\Gamma_s P_{SBS} - P_s g_{SBS} P_{SBS}/A_{eff}. \tag{32}$$

With these adjustments, it might appear that the equations are not coupled. However, the pump powers are coupled to the signal and stokes by N_1 and N_2. Since the signal power will be significantly greater than the SBS power for our model, we will derive the rate equations from the signal power alone. If we assume only one pump direction, then for steady state conditions:

$$N_0 = N_1(z) + N_2(z), \tag{33}$$

$$\frac{dN_1}{dt} = \frac{dN_2}{dt} = 0, \tag{34}$$

$$\Rightarrow \frac{dN_1}{dt} + \frac{dN_2}{dt} = 0, \tag{35}$$

$$\Rightarrow \frac{((N_0 - N_2)\sigma_p^a - N_2\sigma_p^e)I_p}{E_{p(photon)}} + \frac{((N_0 - N_2)\sigma_s^a - N_2\sigma_s^e)I_s}{E_{s(photon)}} - \frac{N_2}{\tau} = 0, \tag{36}$$

where "E" represents the energy of a photon for the associated pump or signal frequency and "τ" represents the lifetime of the upper energy lifetime for the laser. Typical values of "τ" for ytterbium doped fiber amplifiers are around 0.8 ms. Solving for N_2 yields:

$$N_2(z) = N_0\left(\frac{\left(E_{s(photon)}I_p(z)\sigma_p^a + E_{p(photon)}I_s(z)\sigma_s^a\right)\tau}{E_{s(photon)}I_p(z)\left(\sigma_p^a - \sigma_p^e\right)\tau + E_{p(photon)}I_s(z)\left(\sigma_s^a - \sigma_s^e\right)\tau + E_{s(photon)}E_{p(photon)}}\right). \tag{37}$$

Now, dividing by "τ", E_p and E_s, we obtain the following relationships for N_2 and N_1 along the fiber:

$$N_2(z) = N_0 \left(\frac{\dfrac{I_p(z)\sigma_p^a}{E_{p(photon)}} + \dfrac{I_s(z)\sigma_s^a}{E_{s(photon)}}}{\dfrac{I_p(z)\left(\sigma_p^a - \sigma_p^e\right)}{E_{p(photon)}} + \dfrac{I_s(z)\left(\sigma_s^a - \sigma_s^e\right)}{E_{s(photon)}} + \dfrac{1}{\tau}} \right), \tag{38}$$

$$N_1(z) = N_0 \left(1 - \frac{\dfrac{I_p(z)\sigma_p^a}{E_{p(photon)}} + \dfrac{I_s(z)\sigma_s^a}{E_{s(photon)}}}{\dfrac{I_p(z)\left(\sigma_p^a - \sigma_p^e\right)}{E_{p(photon)}} + \dfrac{I_s(z)\left(\sigma_s^a - \sigma_s^e\right)}{E_{s(photon)}} + \dfrac{1}{\tau}} \right). \tag{39}$$

We still need to know the value of N_o in order to solve the rate equations. We can determine N_o from the pump absorption giving by the fiber manufacturer for 915 nm and adjust for 976 nm. The following equation can be used to determine the dopant level N_o:

$$N_o = \frac{\alpha_{effective(dB/m)}}{4.34 \left(\dfrac{d_{core}}{d_{cladding}} \right)^2 \sigma_p^a}. \tag{40}$$

The square of the ratio of the core and cladding diameters adjusts the effective absorption for the portion of pump power entering the ytterbium dopant region. The "4.34" is an adjustment for conversion of dB/m into appropriate units.

To solve the coupled equations, one would need to convert intensities to power units, thus resulting in a "$1/(\tau A_{eff})$" term in the denominator. With this, we now have coupled rate equations for a single pump scheme in either direction. Selection of the best pumping scheme is discussed in section 2.11.

2.9   TEMPERATURE PROFILE IN AN ACTIVE FIBER

As discussed and developed in section 2.7, the acoustic frequency is proportion to temperature, thus resulting in an associated shift in the corresponding Stokes frequency. Recall from section 2.8 that the Stokes power grows exponentially as it beats with the signal frequency. However, a change in temperature due to thermal gradients along the fiber will shift the peak frequency and thus decrease the effective Stokes growth.

Such a thermal gradient can be produced within the fiber core through the nonradiative processes of the simplified two level ytterbium energy processes for amplification. Here the quantum efficiency, η, defined in section 2.2, represents the fraction of pump power transferred to heat[64]. It has been shown that even for high temperature gradients; the radial temperature differential across the core can be neglected, therefore only the temperature differential along the fiber length is considered[64].

In 2001, Brown and Hoffman developed a model for thermal distributions within two distinct radial regions of core and cladding within a fiber[65]. Although there are two cladding layers for dual clad fibers, these were treated as one region with similar thermal conductive and mechanical properties. The outer protective coating is also ignored. The following diagram illustrates this assumption and flow of heat used by Brown and Hoffman:
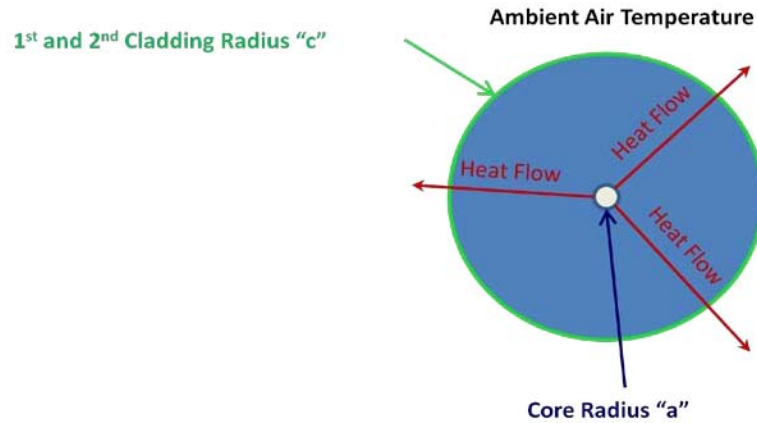
Figure 10: Radial thermal model heat flow

The temperature differential between the core and outside the fiber temperature was evaluated to be:

$$\Delta T = \frac{Q_o a^2}{4k}\left[1 + 2\ln\left(\frac{c_{clad}}{a}\right) + \frac{2k}{c_{clad}h}\right],$$

(41)

where:

Q_o represents the heat density,

k represents the thermal conductivity of the cladding,

a represents the core radius,

c_{clad} represents the total cladding radius,

h represents the convective coefficient.

It must be noted that one must be careful in assigning values for the thermal conductivity and especially the convective coefficient. The coefficient h is the cooling at the fiber surface in contact with stale air. If the air was moving, the value of h should increase. If, however, the fiber was in contact with an insulator, such as a plastic spool, the value of h should go down. For this reason, the results of our active fiber experiments will aide in adjusting our values for h.

Later in 2005, Kovalev and Harrison utilized the results of Brown and developed a relationship for the temperature differential along the length of a dual clad fiber amplifier[64]. Kovalev's relationship concluded, that for constant h along the fiber (cooling conditions are uniform along the fiber), the temperature profile along the fiber will decay exponentially as the pump power. The actual relationship between ΔT and P_p is described below[64]:

$$\Delta T(z) = \frac{Q_o(z)a^2}{2bh} = \frac{\alpha \eta a^2}{2\pi b^3 h} P_p(z),$$

$$\rightarrow Q_o(z) = \frac{\alpha \eta}{\pi b^2} P_p(z),$$

$$(42)$$

where :

b represents the inner clad radius,

h is $\cong$ 1 W/(m^{2}K),

α is converted from dB/m to m^{-1} by dividing by 4.34,

and η is the quantum defect (fraction of absorbed power).

For a counter pump scheme:

$$P_p(z) = P_p(L) e^{[-\alpha(L-z)]}.$$

$$(43)$$

From this we can determine the overall temperature change across the entire fiber. Since the temperature differential follows the pump power, we now have a complete temperature profile along the length of the active fiber according to the following:

$$\Delta T(z) = \left(\frac{\alpha \eta a^2}{\pi b^2 4k} \right) \left[1 + 2\ln\left(\frac{c_{clad}}{a} \right) + \frac{2k}{c_{clad}h} \right] P_p(z).$$

$$(44)$$

With a counter-pump scheme having a signal entrance at distance "0", an illustration of the longitudinal temperature profile is depicted below:

33
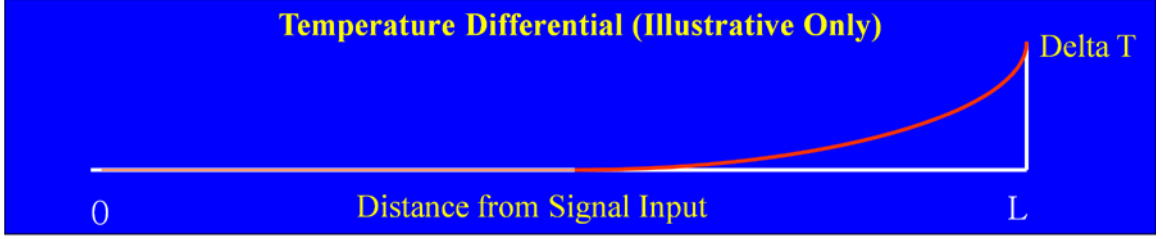
Figure 11: Longitudinal temperature differential in counter-pump fiber

Taking into account the effect of temperature, the following provides the SBS gain coefficient with position and frequency dependence:

$$g_B(v,z) = g_0 \frac{1}{1 + \left[2\left(v - \left(v_B + \left(\frac{\Delta v}{\Delta T}\right)\Delta T(z)\right)\right) / \Delta v_B \right]^2}, \tag{45}$$

where $\left(\dfrac{\Delta v}{\Delta T}\right)$ is the rate of chage of SBS frequency per delta T
and v_B represents the center SBS frequency without a delta T.

In order to account for the temperature effects, we will need to determine the rate of Brillouin center frequency change per degree. The passive fiber experiments will determine this value empirically. The effective SBS gain will be discussed in the model development section of this chapter.

2.10 MODULATION

So far we have looked at how to change the physical characteristics of the fiber to mitigate SBS. Another technique would be to manipulate the incoming laser source so that SBS already present has less of an impact. If the source were broken up into different frequencies with lowered power per frequency, SBS would see each frequency independent of the others. One method might be to phase modulate the source prior to entrance into the fiber.

34

Phase modulation of the pump signal has been shown to increase SBS threshold as well as decreasing the effective SBS gain by changing the phase of the pump wave E-field, thus increasing the effective pump wave spectral width. Lichtman et al. have previously provided preliminary investigation of the effects of modulation on SBS gain [3]. Theoretical results showed that SBS threshold depends on the ratio between the spontaneous Brillouin linewidth and the bit rate for passive fibers used in communications [3]. Lichtman et al. demonstrated that phase modulation would increase the SBS threshold [3].

In an effort to increase SBS threshold for future high power fiber amplifier applications, additional modulation schemes were identified, modeled and tested through this dissertation. Phase modulation of the polarized signal source prior to entering the fiber spreads the input beam spectrum into "side lobes" with overall lowered peak powers. The modulation depth and frequency of the phase modulator determine the number of side lobes and relative peak powers. With a modulation frequency greater than the SBS gain bandwidth, the increase in SBS threshold will be inversely proportional to the decrease in the peak side lobe. The side lode properties were modeled to determine the effect on SBS threshold. The side lobe peak maxima were determined to be proportional to the nth Bessel function evaluated at the modulation depth. These results are shown in Figures 12 and 13 below:
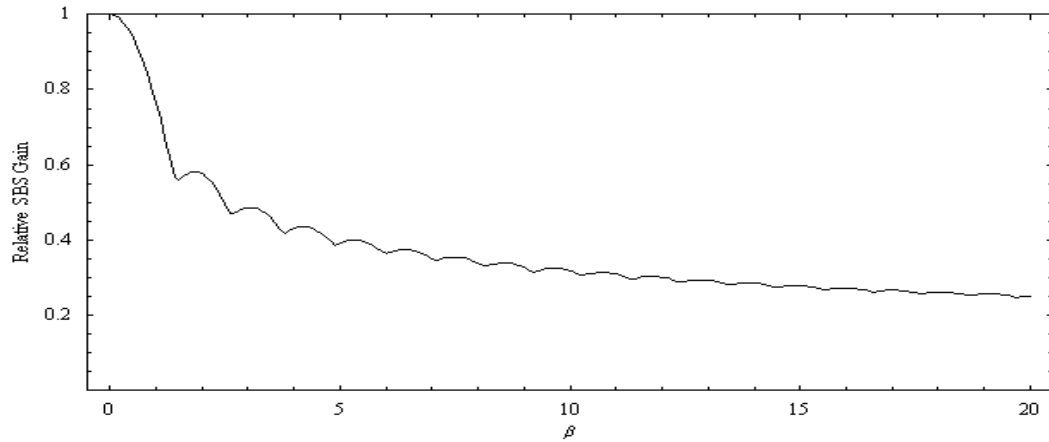
Figure 12: Model of modulation depth versus SBS gain
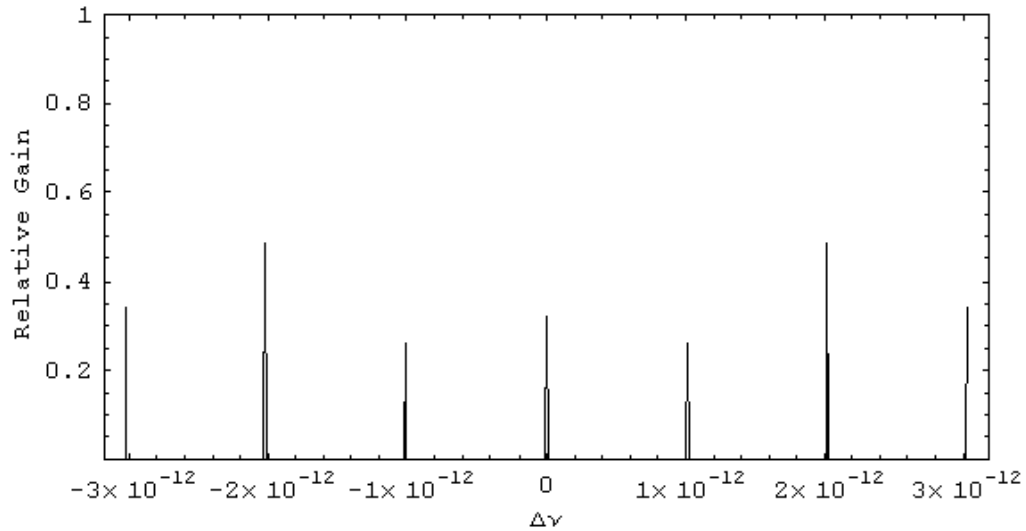
Figure 13: Relative SBS gain-phase modulation of 1 THz and modulation depth ~2.5

The modulation depth controls the peak spectral component of the pump beam and therefore the relative SBS threshold. The smaller the highest peak component the lower the SBS threshold will be also. The relative gain for Figure 13 would be ~0.5, or half the value without modulation. There is a practical limit on the modulation depth, as well as a convergence for the model. For very strong modulation depths, say around 10, one could expect an effective relative gain near 0.25, or an estimated increase in SBS

threshold by a factor of four (4x). A weaker modulation depth near 5 would yield an SBS threshold increase by a factor ~2.5.

Obviously, this model was for demonstrating the effects of phase and depth. A modulation frequency would be more appropriately selected that ensures overlap of corresponding Stokes and signal waves do not overlap.

Using a phase modulator, one might demonstrate a gain reduction in the fiber by spreading the spectrum of the input pump beam. This would create side lobes at the modulation frequency which have a lower overall peak, as shown in Figure 13 above. Assuming the modulation frequency is greater than the SBS gain bandwidth, the reduction in SBS threshold is governed by the amount of power in the most prominent side lobe which is proportional to the nth Bessel function evaluated at the modulation depth. Since each spectral component is outside the gain bandwidth of the others they must create a Stokes signal independently, thus threshold is increased to the point where the peak spectral component reaches threshold. The individual gain components could be "de-modulated" at the exit of the fiber to acquire a single frequency peak power.

2.11   MODEL DEVELOPMENT

In evaluation of the various techniques mentioned for single mode dual clad fiber amplifiers, three possible approaches can be pursued. The first would be for the modeling and development of a single fiber with the highest potential output, the second being a passive combination of these fibers with diffraction limited output, and the third being an active combination of narrow linewidth fiber amplifiers to be used for coherent beam combining. The first two approaches could take advantage of the 2.63 gain in threshold via modulation; however, the third could not since the most recent and viable

active combination requires a separate modulation technique incompatible with a single fiber modulation benefit[50]. All three comprehensive approaches could be used in concert with other techniques for mitigating SBS.

For all approaches, boundary conditions must be set in order to maximize efficiency and effectiveness. Such boundary conditions include overall total length of the fiber, the number of fiber segments, and the maximum pump power. For this effort, such boundary conditions will be based on the existing capabilities, including manufacturability and repeatability, of Nufern DCF amplifiers.

The overall length of the fiber, when SBS suppression techniques are used, is realistically limited by both Stimulated Raman Scattering (SRS) and the absorption characteristics of the ytterbium within the core. Since SRS has a threshold of $\sim 10^3$ higher than SBS, we will initially look at ytterbium absorption characteristics as the limiting factor. For efficiency, we will require that more than 95% of the pump is depleted.

For 95% pump depletion, we must first consider the effective pump power absorption. If the pump absorption is given for a different frequency, then a conversion will be required. The ratio of absorption cross section of the pump frequency divide by the absorption cross section of the given absorption multiple by the absorption value will provide the effective pump absorption form the active ytterbium within the core:

$$\alpha_{effective} = \left(\frac{\sigma^a_{pumpfrequency}}{\sigma^a_{givenfrequncy}} \right) \alpha_{pump\_frequency}. \tag{46}$$

Since the absorption is typically given in dB/m, we will want the total dB absorption to be >95%:

$$\frac{P_p(L_{dis\tan ce})}{P_p(start)} < 0.05, \tag{47}$$

$$dB = 10\log_{10}(.05) = -13.01 dB.$$

Therefore, the model will first perform the following function to determine the overall length to be considered:

$$L_{fiber} = \frac{13.01}{\alpha_{effective}}, \tag{48}$$

where L_{fiber} is given in meters. The initial fiber length will be determined by this method. The number of fiber segments to be used will then be divided by the overall length, giving each the same length as a starting point for the model.

Several factors determine the absorption of pump per unit length, including the ratio of the clad diameter to the core diameter, pump frequency, pump width, and pump stability. In addition, there are competing or complementary suppression aspects associated with the length. Length and temperature differentials as a result of heat from the interactions of the pump with the material are two such characteristics. Specifically, increased absorption permits shorter lengths of fiber resulting in a greater thermal differential along the fiber thus decreasing SBS, as well as decrease the "effective length", thus decreasing SBS as well. Balancing of overall length with the thermal differential created will maximize effectiveness of higher laser output power.

Once the length is determined, the second limiting factor would be the number of fiber segments and the order in which they are placed. Although Nufern was able to produce ytterbium-doped dual clad fiber amplifiers with varying Ge-dopant concentrations, there were manufacturing limits. These limits were based on two factors;

1) the amount of soluble germanium and ytterbium that could be used in the core, and

2) the amount of germanium, fluoride, phosphorous and other elements or compounds used in the cladding to match the numerical aperture uniformity requirement between fibers. With varying concentrations of germanium percent (Ge %) by weight within the core, the cladding material properties had to change accordingly to ensure the same numerical apertures for all fiber segments. In addition, the solubility of ytterbium within the core required the addition of aluminum, thus placing additional constraints on germanium. As a result, Ge % by weight was limited between ~3% - 15%. Other limitations included the accuracy to maintain a specific Ge concentration. Although the requirement was for ~0.35 Ge % between fibers, realistically, we might only be able to acquire ~0.5% between fibers. From this, we are limited to a maximum of about 24-30 fiber segments.

In addition, the order of the fiber segments and the length of each are also critical. Since temperature and % Ge have effects on SBS, we need to ensure that there is no overlap or redundancy. From previous sections, it was determined that temperature and density have inversely proportional effects on SBS. Therefore, to avoid overlap, the lowest density fiber segment must be placed at the highest temperature. Fibers should cascade in order of increasing density as the temperature decrease. Also, the fiber segments will decrease in length as the power continues to increase. Additionally, the gain of the Stokes wave must be considered when developing the overall model, providing an increase of the Stokes power is faster than that of a passive fiber.

The maximum pump power permitted is directly related to the theoretical limit of the material properties of the outer cladding material. As temperatures increase due to

power levels, the outside coating begins to breakdown, thus providing the limiting factor of power per fiber. For our Nufern amplifiers, this power has been estimated to be ~600W-700W by Nufern at the time of purchase. Today, however, improved designs and material properties permit >1.0 kW.

Although these conditions were based on manufacturability and techniques at the time of purchase, we anticipate enhanced supportable manufacturing capabilities to continue. This in turn will permit an additional number of fiber segments to be combined with an estimated increase in SBS threshold. For the single fiber, using these techniques, including modulation, we project a narrow linewidth output power of >1.0 kW with an M^2 <1.5. For beam combining, we anticipate >10 kW power for the passive combination and an estimated >100 kW for the active combination. Even greater single fiber output fibers, resulting in even high combined output power levels beyond 100 kW, could be achieved if combined with other techniques, reaching single fiber output power levels >2.0 kW with M^2 <1.5.

Now, the rate equations developed in section 2.9 are generic for both forward and backward pumping schemes. They do not account for the adjustments required to minimize the effects of SBS on amplification and pumping schemes required for our optimization model. Before we continue, a brief discussion of the appropriate pumping scheme is needed to identify the most effective model.

From the rate equations in section 2.8, we see that the change in the Stokes intensity is proportional to the signal intensity. The pump power falls off exponentially as it propagates along the fiber length, thereby delivering exponentially less "pump" to excite the ytterbium ions within the core along the length of the fiber. Since the gain is

proportional to the number of excited states, the gain will also diminish exponentially. If we pump from the signal entrance end of the fiber, we will have the majority of our gain near the entrance, thus creating a long propagation distance for a higher power signal. On the other hand, if we counter-pump, we will have the majority of the initial fiber length with lower signal power and only create a high power signal for a shorter distance near the end of the fiber. Since SBS threshold is dependent on the signal power and effective length, a counter-pumping scheme will significantly reduce SBS. For this reason, we shall use a counter-pumping scheme for our model. Adjusting our rate equations for this model we now have the following three coupled equations:

$$\frac{dP_s}{dz} = (N_2\sigma_s^e - N_1\sigma_s^a)\Gamma_s P_s - P_s g_{SBS} P_{SBS} / A_{eff}, \tag{49}$$

$$\frac{dP_b}{dz} = -(N_2\sigma_p^e - N_1\sigma_p^a)P_b \left(\frac{d_{core}}{d_{cladding}}\right)^2, \tag{50}$$

$$\frac{dP_{SBS}}{dz} = -(N_2\sigma_s^e - N_1\sigma_s^a)\Gamma_s P_{SBS} - P_s g_{SBS} P_{SBS} / A_{eff}. \tag{51}$$

An additional benefit to the counter-pumping scheme is the associate thermal differential at the end of the fiber where the highest signal power is achieved. The effect of a high temperature gradient near the end of the fiber would further mitigate SBS by shifting the effective Stokes peak frequency response. In order to account for this temperature gradient, our model must develop incremental Stokes responses for each frequency change as a result of this thermal gradient. With the aid of numerical methods, we can separate the responses into discrete intervals of length and sum the overall effects. The SBS will then be a series of discrete Brillouin waves at different peak frequencies

interacting with the signal. Liu has already developed such an approximation and the following rate equations are a compilation of his model with ours[18]:

$$\frac{dP_s}{dz} = (N_2\sigma_s^e - N_1\sigma_s^a)\Gamma_s P_s - P_s \sum_{i=1}^{n} g_{SBS}^i P_{SBS}^i / A_{eff}, \qquad (52)$$

$$\frac{dP_b}{dz} = (N_2\sigma_p^e - N_1\sigma_p^a)\left(\frac{d_{core}}{d_{cladding}}\right)^2 P_b, \qquad (53)$$

$$\frac{dP_{SBS}^i}{dz} = -(N_2\sigma_s^e - N_1\sigma_s^a)\Gamma_s P_{SBS}^i - P_s g_{SBS}^i P_{SBS}^i / A_{eff}, \qquad (54)$$

where P_{SBS}^i and g_{SBS}^i are the i-th Brillouin wave power and gain coefficient for frequency v_{SBS}^i.

Since our model will ensure we are below threshold, we will set the limit on the power ratio between SBS and signal for each fiber segment to be less than or equal to 1%. With this constraint, we can now remove the dependence of SBS on the change of signal power with respect to z. As such, the second term in equation 52 above can be neglected. Each discrete element of SBS power (equation 54) will still interact with the signal power and pump gain giving rise to two exponential Stokes gains, respectively, for an integrated frequency span of responses. The integrated SBS peak frequency, however, will determine the overall SBS power for each fiber segment. The final rate equations now become:

$$\frac{dP_s}{dz} = (N_2\sigma_s^e - N_1\sigma_s^a)\Gamma_s P_s, \qquad (55)$$

$$\frac{dP_b}{dz} = (N_2\sigma_p^e - N_1\sigma_p^a)\left(\frac{d_{core}}{d_{cladding}}\right)^2 P_b, \qquad (56)$$

43

$$\frac{dP_{SBS}^i}{dz} = -(N_2\sigma_s^e - N_1\sigma_s^a)\Gamma_s P_{SBS}^i - P_s g_{SBS}^i P_{SBS}^i / A_{eff}. \tag{57}$$

For noise initiation, we will use a constant temperature of $300\,^{o}K$ since the difference in temperature for determining the initial intensity, even up to $>400\,^{o}K$, has not shown to have any significant effect on SBS. Each fiber segment will assume the same noise initiated intensity at the end of the fiber segment.

The center frequency of each discrete Stokes Lorentzian linewidth response will be downshifted from an initial 16-GHz center frequency located at the end of each fiber segment. A new, calculated total integrated gain coefficient from both the nonlinear gain and ytterbium gain will be used to determine the final P_{SBS} for each of the fiber segments. Initial pump power will be set low enough to ensure threshold is not met for the purpose of determining the appropriate fiber lengths of each segment. The fiber segment with the highest ratio of P_{SBS} to P_s will be decreased by 1.0 cm while the segment with the lowest ratio will be increased by 1.0 cm. The entire process will continue until several iterations reach a reasonable convergence of similar ratios between the SBS power to the signal power.

The final process will determine the SBS threshold power for the overall signal. This will be accomplished by incrementally increasing pump power for the set fiber segment lengths. Once the ratios - as described above - of each of the fiber segments reach .01 or greater, the overall output power of the signal will be assumed to be the threshold power. This will conclude the model process for determining the appropriate fiber segment lengths and the associated threshold output power.

3   PASSIVE FIBER SELECTION AND CHARACTERISTICS

3.1   PURPOSE OF FIBER

For the passive fiber experiments, four fibers were selected in order to assist in the characterization of the effects of temperature and density variations between fibers. The fibers were utilized to acquire baseline measurements for adjusting the model developed in section 2.12. The core diameters and material compositions would be as similar as possible to the ytterbium doped dual clad fiber amplifiers to be used during the active fiber experiments.

In addition, the use of these less expensive fibers will aide in determining the most effective experimental set-up and conditions. The use of passive experiments will de-couple some of the complicated effects associated with active fibers, including gain and temperature differentials. These passive tests, therefore, provide a logical process to gradually increase complexity as each process is well understood and repeatable.

Two fibers, having the same model and standard % Ge concentration by weight within the core, were acquired for the thermal experiments. Uncertainty of the effects to the fiber by the method used for creating thermal equilibrium within the core provided the risk mitigation approach to order one back-up spool. The physical and material properties, including numerical apertures, Ge % by weight, and core/cladding geometries were to be the same as a different manufacturer, Nufern, with the same Ge % concentration for comparison.

The remaining two fibers were selected to conduct experiments for determining the effect of % Ge concentration by weight of the Brillouin center frequency shift. The shift in % Ge was selected in order to observe a significant shift in the center frequencies

by several Brillouin linewidths. The fibers used were standard off-the-shelf products from two of the largest specialty fiber manufacturers to ensure repeatability and reliability of manufacturer specifications. In addition, both companies, Corning and Nufern, make custom designed ytterbium doped dual clad fiber amplifiers.

3.2   CONSTRAINTS AND CONSIDERATIONS

For our thermal effects experiments, the only real consideration was the potential hydrogenation of the cladding by being submerged in a water bath for several hours. Since our measurements were taken within a day or two, this concern was mitigated. The relationship to our active fiber will be closer than unrelated and extrapolated data used by many from 1550 nm wavelength passive fiber experiments conducted in the late 1980s and early 1990s[25, 66].

For the experiments involving the change in % Ge, the most important consideration would be in the relationship to the slightly denser active fibers to be tested later. Utilizing the results from these passive tests will be beneficial for initial model grounding, but adjustments may be required after the active fibers have been evaluated. Also, the additional dopant materials for the active fibers will provide uncertainty in the prediction of the center frequency and linewidth of the Stokes response.

3.3   FIBER CHARACTERISTICS

For the four fibers mentioned above, the following specifications were given:

1. Single Mode Fiber at 980 µm or below cut-off

2. Cladding Diameter (µm): 125 +/- 0.5

3. Core (µm): 5.9 +/- 0.3

4. NA: 0.12 to 0.14

5. Only silica and germanium within the core.

In addition, the two Corning fiber spools to be used for the thermal experiments were to be 500 meters each with a Ge % concentration by weight of approximately 6.0% +/- 0.1%. The Corning fiber to be used for the density variation experiments was to be 1,000 meters with a Ge % concentration by weight of approximately 8.0% +/- 0.1%. Finally, the Nufern fiber to be used for the density variation experiments was to be 1,000 meters with a % Ge concentration by weight of approximately 6.0% +/- 0.1%.

The actual fiber measurements from each of the two companies were as follows:

Table 1: *Passive fiber measured characteristics*

Fiber	Type	% Ge	length (m)	Cutoff	MFD@1060	NA	Clad Diameter
Corning	SM980	6%	500	< 980 nm	6.6 µm	0.12	125 +/- 2 µm
Corning	SM980	6%	500	< 980 nm	6.6 µm	0.12	125 +/- 2 µm
Corning	HI 1060	8%	1000	936 nm	6.1 µm	0.14	125 µm
NuFern	1060-XP	6%	1000	920 nm	6.6 µm	0.12	125 +/- 0.5 µm

All measured characteristics were within the specifications required for our experiments.

4 PASSIVE FIBER EXPERIMENTAL SET-UP

4.1 APPROACH

The overall experimental approach to the development of an SBS mitigation model involves a two-phased engagement: first, to base-line passive single mode fibers for empirical inclusion of the model, and second, to validate and adjust the model with active dual-clad ytterbium-doped fiber amplifiers.

The first phase, the base-lining portion of the experiment, involved three distinct activities that determined the effect of phase modulation, density variations, and temperature variations on the Stokes center frequency and response width. The three activities, in the order they were conducted are as follows:

1. Phase modulation of the source signal with various frequencies and modulation depths.

2. Evaluation of density variations by testing fibers with similar optical, geometric, and material properties with differing core concentrations of percent germanium by weight.

3. Evaluation of the effects of temperature by submerging a single fiber in a water bath that was heated and cooled to acquire uniform fiber temperatures.

Results from these experiments were utilized to adjust the model, and/or gain specific insight, as well as calibration for the dual-clad ytterbium-doped fiber amplifiers.

4.2 BASELINE EXPERIMENTAL SET-UP

For the three activities mentioned above, in an attempt to minimize artifacts due to inconsistent test parameters, the same basic experimental set-up was maintained. The basic experimental set-up is shown in Figure 14.

48

A. Laser Frequency Offset—Lightwave Electronics Laser Offset Locking Accessory (LOLA)

B. Source—Lightwave Electronics NPRO 122 Nd:Yag @ 1.064 um with 200mW output power

C. Probe—Lightwave Electronics NPRO 122 Nd:Yag @ 1.064 um with 300mW output power

D. 25 GHz Detector-New Focus Inc Photodetector Module

E. Variable 1-16 GHz Signal Generator

F. Hewlett Packard 5364A Microwave Mixer

G. Alenia Marconi Systems Phase Modulator, S/N PM.V.A.10.20/ST/F/B 4.8 dB loss

H. ½ Waveplate—Source/Probe Power Control to Detector D

I. ½ Waveplate—Power Control for Probe

J. ½ Waveplate—Power Control for Source

K. Coherent Lab Master Ultima Power Meter for Source (4% pick-off)

L. Coherent Lab Master Ultima Power Meter for Probe Output (4% pick-off)

M. Coherent Lab Master Ultima Power Meter for Source Output (4% pick-off)

N. Test Fiber, Angle Polished Ends (8 deg angle)

O. Objective with Radial Fiber Adjustment and Three Axis Alignment

P. Four Percent "Pick-Off" Mirror

Figure 14: Passive fiber experimental set-up

In this depiction, the red lines represent free space laser paths and the blue lines represent fiber guided laser propagation.

Since the downshifted Stokes frequency of about 16 GHz from the source signal with a corresponding 35 MHz spectral response width would be difficult to measure

directly, a novel methodology for probing the Stokes profile was used. The experimental

set-up shown in Figure 14 above was developed in order to probe the SBS response.

"Probing" was performed by stimulating the source signal, used as a "pump" for the

Stokes response, with a varying frequency laser as the probe. Specifically, two

Lightwave Electronics NPRO 122 lasers were used—laser "B" as the source and laser

"C" as the SBS "probe". The two NPRO lasers were ideal for these measurements since

they remained stable when tuned, had exceptional power stability, and were fairly easy to

use. In addition, they were truly single frequency with an extremely narrow linewidth of

less than 5 kHz. This single frequency output was critical in measuring the Stokes

response to a seed source probe.

In order to control the NPRO laser frequency separation with accuracy and

stability, a Lightwave Electronics Laser Offset Locking Accessory (LOLA) (A) was

used. The source and probe NPRO lasers were focused onto optical isolators (two

isolators in series for the source). The output of these two laser beams were then

propagated through ½ wave plates (H) in order to select relatively equal amplitudes as

they were reflected or "picked-off" and collinearly aligned to a 25 GHz photo detector

(D).

Since the source and probe were separated by a frequency near 16 GHz, the

detector response was that of the associated beat frequency between the two lasers. This

initial beat from the detector was then sent to a frequency mixer (F) where an external

frequency generated by a variable 1-16 GHz frequency generator (E) was combined with

the detector beat frequency. This mixed beat frequency was then sent to the LOLA (A).

The LOLA was set to cancel the mixed beat frequency with a pre-selected 300-500 MHz

reference frequency by changing the probe NPRO laser temperature. The result was a stabilized frequency separation of the two NPRO lasers.

A laptop computer utilizing the software LabVIEW with GPIB interface to the variable 1-16 GHz frequency generator was programmed to scan frequencies near the Stokes response frequency. As the frequency generator increased the frequency signal (initially near 14 GHz), the LOLA balanced the beat to zero by heating the "probe" NPRO laser (C). As the "probe" laser was heated closer to the temperature of the "source" laser, it scanned frequency responses with a known frequency differential from the source. Power meter "L" measured the probe output power. The laptop recorded the probe output power as a function of the calculated frequency separation from the source. The responses and associated peaks represent the Stokes frequencies and relative amplitudes responding to the various source frequencies and amplitudes. This SBS "probe" was the foundation for the entire experimental set-up.

The remainder of the set-up was used to control the power and polarization for both the source and probe legs of the propagation. The probe is on the bottom portion of the set-up while the source is on the top portion.

After the probe exited the "pick-off" mirror for the "beat" portion of the experiment, it propagated through a polarizing beam splitter (PBS-used for another experimental set-up) and then enters a ½ wave plate (I). This ½ wave plate is used to adjust the overall probe power entering the test fiber. The laser then propagated through another PBS and the vertical polarization is then reflected 90 degrees right to the incident.

This particular PBS was used to measure the output power from the source. Specifically, it is used to adjust the following in-line ½ and ¼ wave plates to either ensure co- or cross-polarization of the probe to source. Minimizing the source power at this location of the PBS by adjusting the ½ and ¼ wave plates would ensure co-polarized alignment with the probe. Maximizing the source power at this location, on the other hand, would ensure cross-polarization with the probe. This allowed for control of the polarization so gain measurements could be collected with the probe beam both co- and cross-polarized with the source.

The probe continued to propagate and reflect off of a mirror through the ½ and ¼ wave plates, respectively. The probe continued through the pick-off mirror (P) and then into an objective (O). The objective focused the probe into the test fiber (N).

It must be noted that all free laser propagations were focused onto fibers using an objective and a three axis adjustable configuration. Newport Electro-Strictive AD-30 Actuators adjusted by Newport u-Drive Controllers, Model ESA-C, were used to provide steady and stable alignment of all fiber ends. Connectors with an 8.0% angle polish were placed on all test fiber ends.

For the source leg, the beam propagation out of the beat pick-off mirror continued through a ½ wave plate (J) used to adjust the overall source power entering the test fiber. The laser then propagated through a PBS and the vertical polarization was reflected 90 degrees right to the incident. This polarized beam was then reflected approximately 90 degrees to the left of incident off of a mirror and into a second ½ wave plate. This second ½ wave plate was used in tandem with the first to ensure proper polarization alignment and power input into the polarization maintaining (PM) fiber used for the

phase modulator (G). The source was focused onto the PM fiber of the phase modulator which propagated through the phase modulator and existed through another objective lens (O). The source beam then propagated through another pick-off mirror (P) and entered the test fiber (N) through an objective lens (O). This completed the entire experimental set-up and source/probe propagation for the passive "base-lining" portion of the experiment.

The phase modulator in the upper portion of Figure 14, although in place for all passive fiber experiments, was actively used only for the portion of the experiment investigating the effects of phase modulation on the SBS gain.

4.3   PHASE MODULATION VARIATION

The phase modulation experimental activity utilized the baseline experimental set-up discussed in section 4.2, with the exception that the phase modulator was active during this portion of the passive fiber experiment—except for the initial measurement without the phase modulator active. The transmitted Stokes (probe) and pump (source) powers were measured with relationship to the wave plate angles to ensure co-polarization. Without the source, the transmission of the probe power was set so that approximately only 1.03 mW was transmitted through the test fiber. The baseline frequency difference between the probe and pump was 15.370 GHz (frequency generator setting). The LOLA offset was set to 500 MHz. The center frequency of the Stokes response was therefore 15.870 GHz. The SBS gain profile was measured within this region for all phase modulation test runs.

The first run scanned off-set frequencies without the phase modulator active and recorded the Stokes (probe) power as a function of the off-set frequency. There were

four additional runs with an active phase modulator. For these runs, the phase modulator was driven at 100 MHz, 200 MHz, 300 MHz, and 400 MHz. Each was driven with a 40 dB amplifier and a setting of -18 dBm on the signal generator. The results were recorded, plotted and presented in section 5.1 of this report.

Additional experiments were run to determine the overall effect of the modulation depth on the peaks of the Stokes "side lobes" created by the modulator. These measurements were recorded and are presented in section 4.1 as well.

4.4   GE-DOPANT VARIATION

For the evaluation of density variations on the acoustic velocity, measured by the shift in the Stokes response, two fibers were used. The first fiber tested was 1000 m of single mode, 5/125, Nufern 1060-XP with a 6.0% germanium weight concentration within the core. The second fiber tested was 1000 m of single mode, 5/125, Corning HI 1060 with an 8.0% germanium weight concentration within the core. In addition to these two direct tests, 500 m of single mode, 5/125, Corning SM980 with a 6.0% germanium weight concentration within the core was used during the thermal effects portion of the passive fiber experiment as a comparison with the Nufern fiber.

For each fiber, the SBS probe was utilized, as described in section 4.2, to measure and record the probe relative power as a function of frequency separation from the source. Several runs were made for each fiber to verify consistency. Additional measurements were also taken to observe any polarization dependency effects—cross- and co-polarization alignment of the probe with the output of the source. The results of these two fibers, as well as the results of the 500m of SM980 fiber at room temperature, are presented in section 4.2.

54

4.5   THERMAL EFFECTS VARIATION

The measurement of temperature effect on the acoustic velocity was indirectly measured by measurement of the Stokes response using the same SBS probe discussed in section 4.2. Corning's single mode SM980 fiber, 500 m, was used for these tests. Since the time to achieve thermal equilibrium of the fiber in air was estimated to be ~10-20 hours for each measurement, combined with limitations of lab equipment to produce a well insulated furnace, it was determined that water as a thermal medium would be a practical alternative. The challenge was to take several readings before the fiber became hydrogenated to a degree that would affect the optical properties. Other than delamination of the coating, it was estimated that the fiber could be submerged for several days without detrimental effects.

A picture of the actual experiment during analysis is shown in Figure 15.
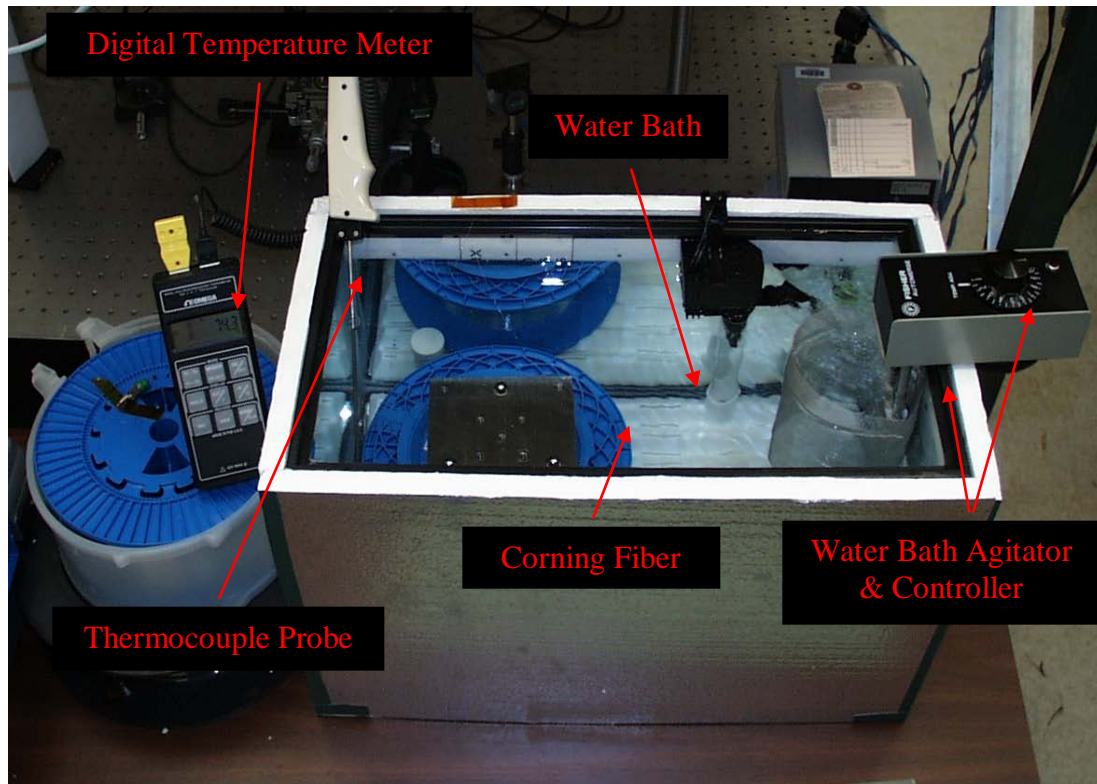
Figure 15: Thermal effects experimental configuration

To ensure consistent temperature over the time required to probe each temperature, a typical small fish aquarium surrounded by insulating Styrofoam was used as the container. Temperature equilibrium throughout the tank was achieved utilizing the water bath agitator and controller as indicted in the figure. A digital temperature meter connected to a thermocouple probe submerged in the water bath, also shown, was used to measure the bath temperature—the fiber temperature at equilibrium.

From those who scuba dive, it is known that water transfers heat about 20 times more effectively than air. The time for the fiber to reach equilibrium with the water bath temperature, therefore, was estimated to be about 30 minutes. The bath was initially cooled to ~32 degrees Fahrenheit with ice cubes. A measurement was taken after about 30 minutes. The temperature was allowed to slowly rise to room temperature taking

measurements along the way, using ice cubes to stabilize the temperature long enough for the fiber to equilibrate to the water ambient temperature. Once the rising temperature was stable again, another measurement was taken.

As the temperature passed room ambient temperature, a heater was used to increase and maintain the temperature. This continued until the maximum temperature of about 180 degrees Fahrenheit was achieved. The entire bath was then permitted to cool to room temperature as additional measurements were taken. Ice was once again added to continue measurements below room temperature. The results of these measurements are presented in section 4.3.

5   PASSIVE FIBER RESULTS

5.1   PHASE MODULATION

Phase modulation experiments were conducted as described in section 3.3. These

experiments demonstrated SBS suppression in single mode fibers with a decrease in

Brillouin frequency output by nearly a factor of four through phase modulation of the

pump signal. For these experiments, the source was modulated with modulation

frequencies of 100, 200, 300 and 400 MHz and compared to no modulation with a

common "strong" modulation depth. An SBS seed signal was beat against the source to

ensure separation of frequency. As the seed signal laser was heated closer to the source

laser, it scanned frequency responses with a known frequency differential from the

source. The responses and associated peaks represent the Stokes frequencies and relative

amplitudes responding to the various source frequencies and amplitudes. The results are

shown in Figure 16:
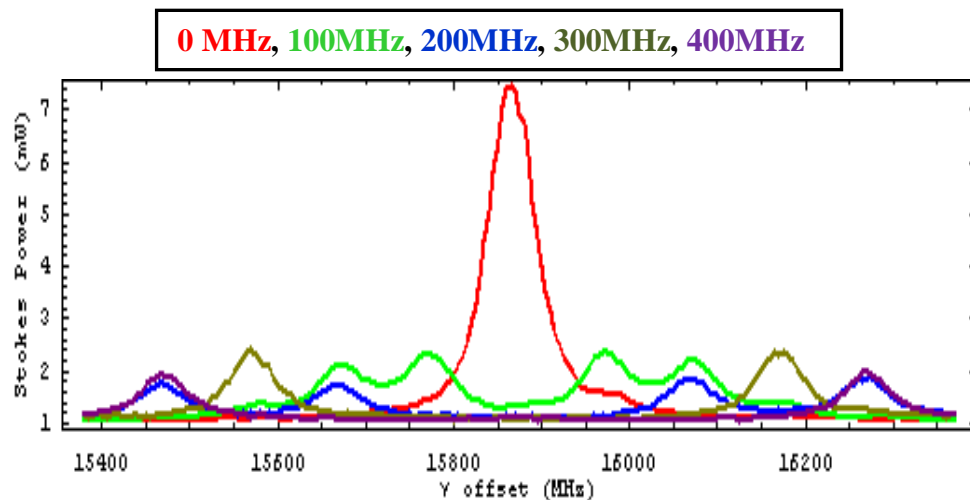
Figure 16: SBS seed response to phase modulation

Using a lithium niobate phase modulator, we were able to demonstrate a gain reduction in the fiber by spreading the spectrum of the input pump beam. This created side lobes at the modulation frequency which have a lower overall peak. Assuming the modulation frequency is greater than the SBS gain bandwidth, the reduction in SBS threshold is governed by the amount of power in the most prominent side lobe which is proportional to the nth Bessel function evaluated at the modulation depth.

The results of the strong modulation indicate a reduction of SBS by nearly a factor of four. Specifically, the non-modulated power peak was ~7.25mW and the modulated side lodes for the various frequencies were ~2mW. The normalized modulated peak values are then ~.28. This is in agreement with the model predictions for a modulation depth near 10. The model predicts convergence of effects as the strongest modulation depths approach peaks of ~.25 that of the original signal.

Again, to ensure benefits of such a scheme, corrective modulation scheme is required at the output. Although this technique works, the added requirement to decouple the modulation, combined with the inability to coherently beam combine, we will only use this method for single fiber development.

5.2   GE-DOPANT PERCENT BY WEIGHT EFFECTS

Two fibers by two separate vendors, differing only in germanium weight concentration, were tested utilizing the set-up and method described in section 4.4. The first fiber tested was 1.0 km of single mode, 5/125, Nufern 1060-XP with a 6% germanium weight concentration within the core. The second fiber tested was 1.0 km of single mode, 5/125, Corning HI 1060 with an 8% germanium weight concentration within the core. In addition to these two direct tests, 500 m of single mode, 5/125,

Corning SM980 with a 6% germanium weight concentration within the core was used

during the thermal effects portion of the passive fiber experiment as a comparison.

Variations in the Ge dopant concentrations within the core of single mode fibers caused

large variations in the SBS gain measurement as shown in Figure 17:

Table 2: *Stokes shift and bandwidth--different Ge-dopant % weight fibers*

Dopant (%Weight Ge)	Center Frequency (GHz)	Bandwidth (MHz)
8	*15.7268*	*23.7*
6	*15.9051*	*34.0*
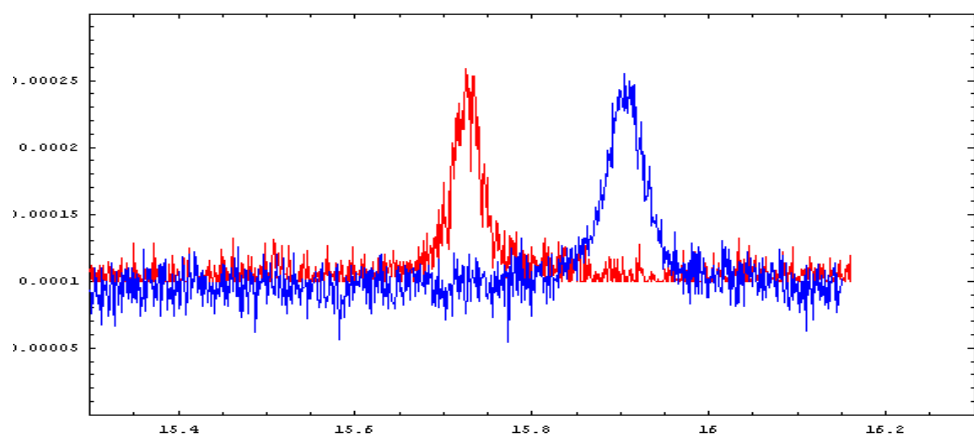
Figure 17: SBS absorption of two SMFs-dopant variation

Both the Corning and Nufern fibers had nearly identical numerical apertures, but

had a 2% variation in the Ge dopant for percent weight. The Stokes shift changed by

nearly 200MHz between the two fibers that is several times the SBS gain bandwidth of

approximately 35 MHz. The Corning SM980 used in the thermal experiment at room

temperature with 6% germanium weight concentration had nearly identical SBS center

frequency and bandwidth as the Nufern 6% germanium weight concentration. The

overall effect of the change in density resulted in 89.15 MHz shift per 1.0 % Ge by

weight concentration differential.

It must be noted, however, that the bandwidth of the differing germanium concentrations varied significantly, with the 8% being ~24 MHz while both the 6% fibers being ~34 MHz. It appears that the SBS bandwidth may be significantly dependant on the process and/or concentrations. Care must be taken to avoid assuming that custom dual clad fibers will have consistent bandwidths, especially for varied germanium dopant concentrations. With the addition of ytterbium, the SBS bandwidths may also be significantly different than those observed for these passive fibers. Measurements should be made for a single active dual clad fiber to verify the SBS bandwidth.

5.3 THERMAL EFFECTS

Temperature effects on the SBS center frequency were measured for 500 m of single mode, 5/125, Corning SM980 with a 6% germanium weight concentration within the core. Several experimental runs were conducted and all achieved consistent results. It was determined that that a change in temperature of one degree Fahrenheit results in a shift in the Stokes frequency by 0.93 MHz as shown below:
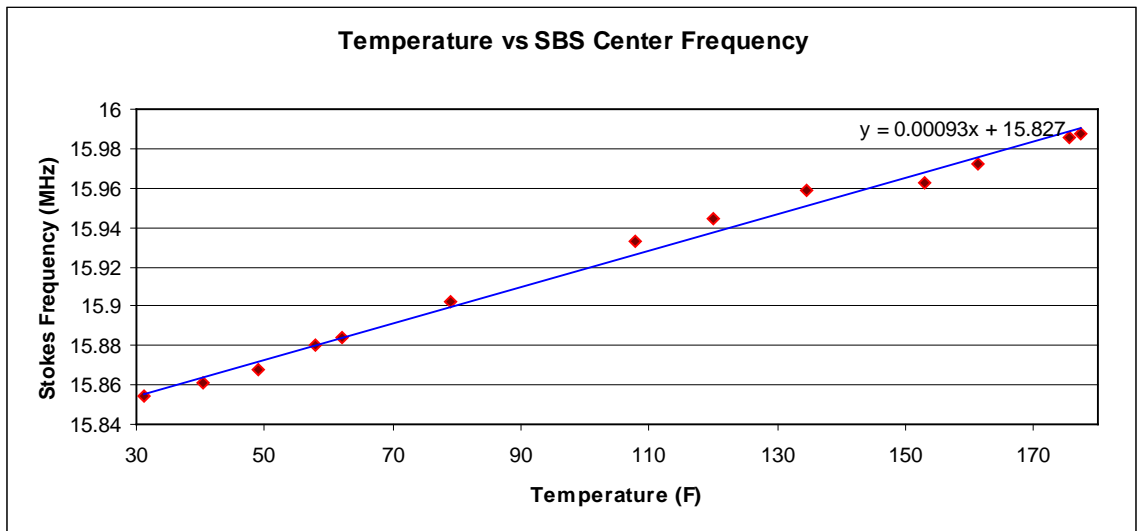
Figure 18: Effects of temperature on stokes frequency on SMFs

Since typical passive fiber SBS widths observed are about 35 MHz, a temperature differential of 38 degrees will shift the Stokes frequency outside of the previous response. The increase in the Stokes center frequency with temperature is consistent with our original model where the acoustic velocity is proportional to temperature. Again, the effects of temperature on SBS are dependent upon the SBS bandwidth and frequency of the particular fiber.

6   MODEL ADJUSTMENTS

Taking into account the results of the effects of temperature on the center Brillouin frequency for passive fibers, we will now use 0.93 MHz/^{0}F or 1.67 MHz/^{0}K as the dependence of temperature on Brillouin frequencies. Also, with the additional dopants used for the active fiber medium, the linewidth of the active fiber Brillouin response will probably increase, so we will use a value of ~40 MHz, vice the 34 MHz observed for passive fibers, for the active fiber. The effect of % Ge concentration by weight on the Brillouin center frequency was 89.15 MHz per 1.0% Ge shift. Therefore, in order to acquire at least a Brillouin shift between fiber segments, we will use a change of 0.5% Ge concentration by weight for the active dual clad ytterbium doped fiber amplifiers.

For the actual design, we will set the total fiber length at the 95% absorption length for the pump power. In addition, we will use a counter-pump pumping scheme. Finally, the position of the segments will be increasing in % Ge concentration from the signal input to account for the thermal gradient of the counter-pump scheme.

7   ACTIVE FIBER SELECTION AND CHARACTERISTICS

7.1   PURPOSE OF FIBER

Similar to the passive fiber selection, the active dual clad fibers were designed to evaluate the effect of density and temperature variations on active ytterbium-doped dual clad fiber amplifiers. The fibers developed were also selected to test the manufacturability of differential germanium-dopant concentrations to within a 10% deviation from specifications. Standard and consistent Nufern dual clad fiber parameters were used, including: percent weight of ytterbium, numerical apertures, geometries, cladding and coating materials, draw processes, and architectures.

Two custom fibers were purchased, each with differing germanium concentrations near the same germanium densities and core diameters used by the passive fibers for comparison. Based on the results of the passive fibers, the specific percent weight of germanium was chosen to ensure a visible separation between SBS gain peaks. As discussed in section 5, a 0.5% Ge by weight was selected between the two dual clad fibers versus the 0.35% Ge required by the passive fibers. The additional 0.15% Ge by weight was chosen to account for any uncertainty in manufacturability and densities of the core.

7.2   CONSTRAINTS AND CONSIDERATIONS

As with many applications of science, there are limiting factors, or constraints and practical considerations which limit the ability to utilize all positive attributes of our model. Using common fiber manufacturing techniques, typical dopants added to raise the index include germanium, aluminum, and phosphorous [41]. The only common dopant used to lower the index is fluoride. Within the core, GeO_2 is typically added to raise the

index necessary to acquire appropriate numerical apertures because of the concentration limitations by other dopants within the gain medium. Adding GeO_2 also raises the overall density of the core, a benefit to changing the acoustic velocity and associated Brillouin center response frequency. Because of the ability to add a significantly large percentage by weight of GeO_2 to the core, the only changes to the core material composition for this dissertation will be % Ge by weight. In order to maintain consistency of numerical apertures among the fiber segments, the first clad will have varying dopant concentrations of germanium, phosphorous, and fluoride to raise or lower the 1st clad index appropriately.

The germanium dopant concentration within the core, utilizing today's manufacturing capabilities, however, has limitations. Specifically, the variation of percent (%) weight Ge within the core is limited by the demands of lower numerical aperture. With a numerical aperture of 0.14 and associated core diameter of about 5.0 um, the core germanium concentration can be varied from about 2%-18% - resulting in as many as 40 individual fiber segments (according to Nufern representatives). This is not true, however, for larger cores. According to a manufacturing representative at Nufern, it becomes extremely difficult to vary the germanium concentration for larger core diameters-a property that requires a decrease in the numerical aperture in order to maintain single mode propagation. Recall that the V-value must remain below 2.405 for single mode operation. Since V is proportional to the core diameter and the numerical aperture, an increase in the core diameter must be compensated by a decrease in the numerical aperture.

$$V = \frac{\pi \times d_{core} \times NA}{\lambda} \leq 2.405 \text{ (for single mode)}. \tag{58}$$

The numerical aperture is also proportional to the index of refraction and the acceptance angle:

$$NA = Sin\theta_{max} = \sqrt{n_{core}^2 - n_{1st\_clad}^2} \ . \tag{59}$$

For current manufacturing techniques, the first and second cladding material properties are designed to ensure multimode acceptance of the pump diode within the inner clad, typically with a numerical aperture ~0.46. If the relative first clad index remains the same, then the core index must decrease with a decrease in the numerical aperture. For this reason, an increase in the core diameter, resulting in a decrease in the numerical aperture, requires a decrease in the core index of refraction. However, as the index of refraction becomes smaller, the variation of germanium dopant concentration within the core has a greater effect on the index and associated clad dopant requirements. Maintaining the core numerical aperture requires the germanium dopant concentration to be significantly constrained to only a few percentages for current clad architecture designs. Furthermore, if we permit a larger index value for the core, an associated larger clad index is required as well. As a result, fusion splicing becomes more difficult due to the greater density of the cladding resulting in a differential melt temperature between the two fiber-clad segments. For this reason, the increase in core diameter has both physical and practical limitations to the overall suppression of SBS because of the limiting number of segments that could be made.

As an example, Table 3 is an estimate by Nufern of the core index difference, core diameter, numerical aperture, mode field diameters at 1060 um for dual clad ytterbium doped fibers similar to the ones used for this experiment. The figure below presents two graphs showing the associated effects on NA and index of refraction difference as the core diameters changes. As the core diameter increases, both the NA and index begin to converge on single values respectively.

Table 3: *Effects of core diameter on index and NA*

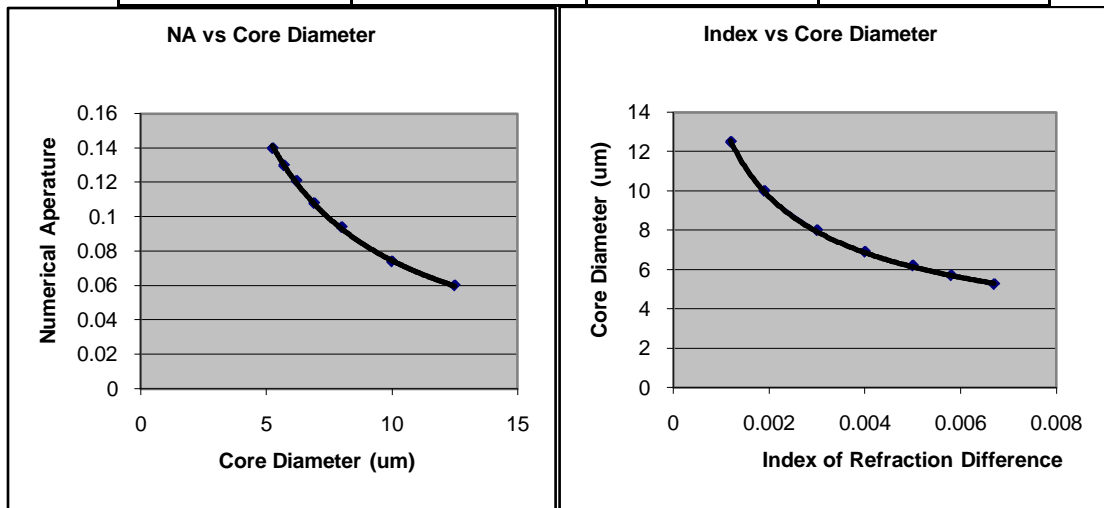| Index Difference	Core Diameter (µm)	NA	MFD @ 1060 (µm)
0.0012	12.5	0.060	14.7
0.0019	10.0	0.074	11.7
0.0030	8.0	0.094	9.3
0.0040	6.9	0.108	8.0
0.0050	6.2	0.121	7.2
0.0058	5.7	0.130	6.7
0.0067	5.25	0.140	6.2

Figure 19: NA and index versus core diameters

For our model, it is assumed that future manufacturing capabilities and architectures will overcome many of these initial core index constraints. Based on this

assumption, the model will be capable of adjusting the core sizes with an NA ~.06 such that at least a 10% variation of germanium concentration within the core will be available.

To further constrain our model, there is also a practical limit to the numerical aperture. Around or below a numerical aperture value of ~0.06, the fiber begins to exhibit extremely high sensitive bend loss and it is also difficult to control the index of refraction in conventional fibers to reliably achieve lower NA's. Utilization in aircraft and other more severe environment applications would require minimal bend sensitivity. For these reasons, we will limit our model application to those fibers with numerical apertures of 0.06 or greater.

According to a Nufern representative, current standard manufacturing capabilities limit the ytterbium dopant concentration within the core to less than 2.0%, with the most common concentrations near 1.0%. The addition of ytterbium dopant also places constraints on the core diameter, similar to the discussion presented above. For this reason, the ytterbium dopant concentration for the model will be limited to 1.5% to ensure practical application. Given the octagonal clad geometry for our fibers, the pump power is distributed uniformly within the core such that pump absorption is proportional to the ratio between clad and core diameters. Increasing the ytterbium dopant concentration within the core will provide proportional increase to the absorption and associated gain according to the following:

$$ABS_{New} = \left(\frac{AreaCore_{New}}{AreaCore_{Old}} \right) x \left(\frac{AreaClad_{Old}}{AreaClad_{New}} \right) x ABS_{OLD} x \left(\frac{Conc_{New}}{Conc_{Old}} \right) \qquad (60)$$

Where ABS_{New} is the predicted absorption in dB/m, ABS_{OLD} is the previous absorption in dB/m, *AreaCore* and AreaClad with subscripts "*Old*" and "*New*" represent the core and cladding cross section areas of the previous and desired core and cladding areas in m² respectively, and $Conc_{New}$ and $Conc_{Old}$ represent the previous and new ytterbium dopant concentrations within the core as percent weight of ytterbium.

If we maintain the core and clad geometries, the absorption will increase by 50%, thus decreasing the overall length of the fiber by 1/3. However, if we maintain the original ytterbium concentration and first clad dimensions, but increase the core diameter to 12.5 um, the absorption will increase by a factor of ~2.4. Together, these two simultaneous changes will result in an overall decrease of the required fiber length by a factor of ~3.6. This decrease in fiber length will significantly reduce SBS.

Notice that we use the actual dimensions of the fiber for the estimated absorption, but we use the mode field diameter for the affected area for SBS. Utilizing the mode filed diameter of 14.7 um rather than 6.2 um increases the effective area for SBS by a factor of ~5.6. Therefore, by increasing the core diameter to a reasonable value, with a 1.5% ytterbium dopant concentration, providing future manufacturing capabilities and associated splicing for this are possible, we can increase our SBS threshold by a factor of ~20. If we also include the ability to permit a 10% variation of Ge concentration by weight within the core, assuming 2 segments per 1%, we have the potential to observe an increase in SBS threshold by an overall factor of ~400. Again, the caveats are that 1.5% ytterbium concentration solubility within the core is possible while changing the core density by 10% and adjusting the cladding dopants appropriately to maintain the same numerical aperture between fiber segments. Excellent manufacturing controls would be

required for this approach. Validation of a manufacturer's capabilities to produce such fibers would be required.

This will be limited further due to splice losses and the actual linewidth of the Stokes response within the active fiber. The number of splices will also be limited by the minimum length required to fusion splice two segments. According to Nufern representatives, fusion splice loss for similar dual clad ytterbium fibers is about 0.03 dB. The minimum length required to make a splice is about 20 cm. Therefore, our model will only use segments > 20 cm.

If the 1st clad is the only material to change in material composition-other than germanium-in order to maintain the NA for the same size cores, we must consider the effects of index on the fiber segments of differing Ge % by weight. Significant changes in index will also affect SBS, but more importantly, create potential reflections at the interfaces between fibers. For a 1.0 wt% GeO2 = 0.577 mol% GeO2 there will be a 0.00084 increase in refractive index over pure silica.

% Ge Dopant vs Increase in Index of Refraction
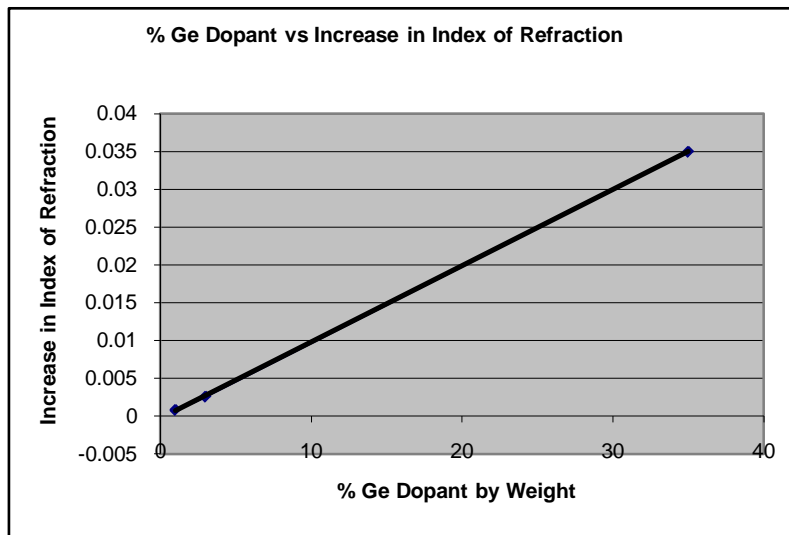
Figure 20: Effect of germanium on refractive index

Utilizing fiber segments with a 1/3 % Ge by weight differential, and an estimated core index ~1.5, we have a difference in index between fibers < 0.02%. The reflectivity of the power is:

$$R_{power} = \left(\frac{n_{segment1} - n_{segment2}}{n_{segment1} + n_{segment2}} \right)^2.$$ (61)

The resulting power reflectivity at the splice for these assumptions will be ~9 x 10^{-9} –negligible for our model.

Also the effect on SBS, more specifically the Brillouin center frequency as developed in section 2, is given by:

$$\nu_B = \frac{2nV_{Acoustic}}{\lambda}.$$ (62)

For a typical 1064 nm wavelength, the Brillouin center frequency, ν_B is ~16 GHz. A change of 0.00028 in index of refraction between adjacent fibers will result in ~ 3 MHz shift in the center Brillouin frequency-an order of magnitude smaller than the SBS linewidth. Since the fiber segments are shifted an entire SBS linewidth due to the density differential, the shift due to the change in index between fiber segments is a negligible effect for our model.

7.3   FIBER CHARACTERISTICS

Three specialty dual clad ytterbium-doped fiber amplifiers were specified and purchased to support this dissertation. The fiber specifications were based on current capabilities of fiber manufacturers in 2002. Nufern was selected based on price and availability. The specialty fiber specifications were as follows:

Table 4: *Active ytterbium-doped fiber specifications*

Product	Fiber 1	Fiber 2
Length (m)	>=50	>=50
Cutoff (nm)	920 +/- 50	920 +/- 50
MFD (μm)	6.2 +/- 0.3 @ 1060nm	6.2 +/- 0.3 @ 1060nm
Coating Type	dual acrylate, UV curable	dual acrylate, UV curable
Operating Temp. Range	-60°C to 85°C	-60°C to 85°C
Numerical Aperture - Core	0.14	0.14
Numerical Aperture – 1st Clad	0.46	0.46
Core Composition	GeO_2, P_2O_5*,SiO_2*	GeO_2, P_2O_5*,SiO_2*
% Ge by Weight	6.0%	5.5 %
Cladding Composition	SiO_2	F, SiO_2
Yb dopant level	>1 wt% **	>1wt% **
Peak Absorption @ 915 nm	0.20 dB/m	0.20 dB/m

*P_2O_5 and SiO_2 concentrations constant & the same for each fiber core
** Yb concentrations must be constant & within 10% variance for each fiber

As mentioned previously, the fibers were selected to ensure comparison with the passive fibers, while maintaining at least a Brillouin linewidth separation from each other. Since 6.0 % Ge concentration by weight was used for the passive fibers, this was the base value selected. For a full Brillouin frequency shift between fibers, a delta of 0.5% below base value was chosen, that is 5.5% Ge concentration by weight.

The following are the actual measured results of the final two fibers manufactured:

Table 5: *Characteristics of purchased ytterbium-doped fiber amplifiers*

Fiber #	Core NA	Clad NA	%Ge	Peak Absorption	MFD	%Yb	Flat to Flat	Attenuation
1	0.146	0.46	6.01	0.20 dB/m @ 915	6.07 @ 1060	~1.0	200 µm	4.2 dB/km
2	0.1444	0.46	5.43	0.21 dB/m@915	6.17 @ 1060	~1.0	200 µm	3.9 dB/km

The coating/2nd clad diameter was measured at ~350 um. The following figure illustrates the relative dimensions and shape of the fibers:
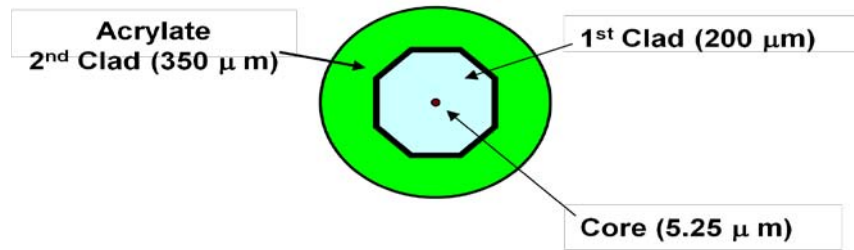
Figure 21: Dual-clad fiber diagram

The real difference from the specification to actual was in the fabrication process where each core had equal amounts of aluminum and ytterbium, but varying amounts of silica, germanium, phosphorous, and fluoride within the first cladding to ensure consistent core numerical apertures between fiber segments. Variations of index of refraction between the fibers were also measured. The differences were similar to those mentioned have negligible effects on our model. All relevant specifications were met within or near 10%. The fibers were manufactured in 2002, There have been significant advancements in dual clad fiber manufacturing capabilities over the past six years, meeting future, more stringent specifications should not be a challenge at the present time.

8 ACTIVE YTTERBIUM-DOPED FIBER EXPERIMENTAL SET-UP

8.1 APPROACH

This portion of the experimental set-up was utilized for the model validation and adjustment as mentioned in section 4.1. The active fiber experiment included the analysis of a single dual-clad ytterbium-doped fiber amplifier while being pumped (active), followed by the analysis of three cascading (active) dual-clad ytterbium-doped fibers with various acoustic velocity responses (varying Ge dopant concentrations). These three fibers varied in length and were cascaded in a manner to minimize SBS threshold effects. The final analysis of the two cascading dual-clad ytterbium-doped fibers included a modified experimental set-up to provide a passive and active mapping of the comprehensive Stokes spectral response utilizing the SBS probe method described in section 4.2. This final analysis was used to validate and modify the longitudinal temperature model, Ge dopant dependence, and other aspects of the model developed in section 2 and adjusted in section 5.

8.2 ACTIVE YTTERBIUM-DOPED FIBER BASELINE EXPERIMENTAL SET-UP

For the active fiber experiments, a few adjustments were made to the passive fiber experimental set-up in order to accommodate the pumping and monitoring requirements. The phase modulator was removed and a 4% pick-off mirror (P) to measure the probe output power along with a dichroic mirror (S) to extract the residual pump power was inserted in its place. Additionally, an Alfalite pump laser (T), used to counter-pump the

dual-clad ytterbium-doped fiber amplifier, followed by an objective (O) and power meter (U), were also added. Two additional power meters (V and W) were positioned to measure the residual Alfalite pump power and 4% of the Stokes power (probe), respectively.

For the first two portions of the active fiber experiments only the "source" laser was utilized. For this reason, only the source laser propagation is inducted with a red line in Figure 22:

S.   Dichroic Mirror—Picks-off residual 976 pump from Alfalite

T.   Alfalite AC2-976-31-213 976 nm 21 Watt Pump

U.   Coherent Lab Master Ultima Power Meter for Source Output

V.   Coherent Lab Master Ultima Power Meter for Pump Residual Output (dichroic pick-off)

W.   Coherent Lab Master Ultima Power Meter for Probe Output (4% pick-off)

X.   2 ½' OZ Optics PM SMF Pigtail with Manufacturer 8 Degree Polished Connector

Y.   Neslab KRDLOA005 Refrigurated Recirculator Chiller RTE-140
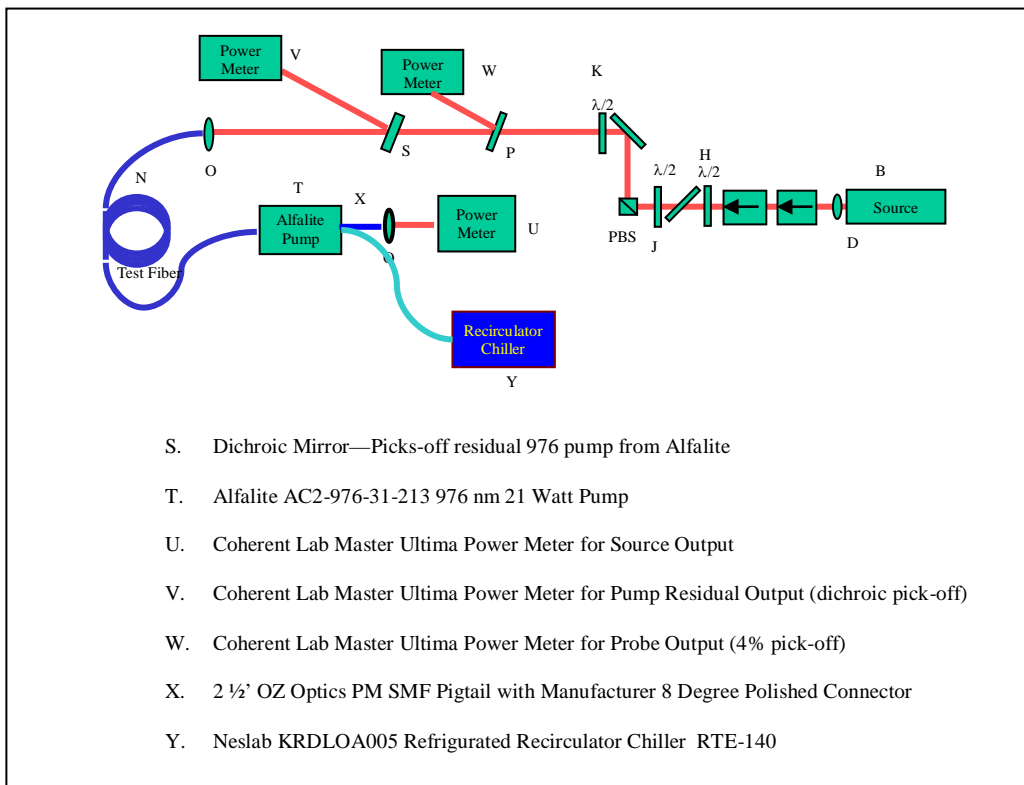
Figure 22: Active fiber baseline experimental set-up

The 976 nm wavelength Alfalite pump was set on a cooling plate to provide a heat sink for to aide in frequency stability. The plate maintained a constant, colder temperature through the circulation of refrigerated water through an enclosed channel within the plate. The water was re-circulated using a temperature controlled chiller (Y).

The frequency stabilization of the Alfalite system was estimated to be within 1.0 nm of 976 nm.

The input of the Alfalite was fusion spliced to 2 ½ feet of an OZ Optics Polarization Maintaining SMF Pigtail with a manufacturer 8 degree polished connector. Alignment was straight forward since the Alfalite input had the same core-cladding dimensions as well as similar polarization maintaining stress rod geometries. The estimated loss within the core due to the fusion splice was about 0.01 dB.

Calibration of the Alfalite was required to accurately determine the initial pump power insertion. A current-voltage driver was used to control and vary the Alfalite pump power. To determine the pump power response to current, the current was incrementally increased while measuring the pump output power. Three runs were conducted to ensure consistency at the same chiller temperature. A plot of current versus pump power was created for future reference and conversion.

8.3 SINGLE ACTIVE YTTERBIUM-DOPED FIBER VALIDATION EXPERIMENTAL SET-UP

Based on the model and previous experimental results, the Nufern fiber with the lowest density core (5.43 % weight of germanium) was selected for the single active fiber test. In this manner, the increasing temperature differential along the fiber length would complement the effects of the decreasing fiber densities between the two cascading fibers—an additional fiber would be fusion spliced to this fiber for the next set of experiments. The total fiber length selected was twenty meters in order to absorb over 95% of the pump power. The total length of the following experiments using cascading fibers was also twenty meters to provide relevant comparisons.

Since the Alfalite fiber pigtail inner cladding diameter (125 µm) was 75 µm less than the Nufern fiber inner cladding diameter (200 µm), Alfalite pump power insertion into the Nufern fiber was not considered to be an issue. However, the differential in cladding geometries made it difficult to acquire an exceptional fusion splice. The resulting loss within the core at the fusion estimated by the fusion splicer was 0.1 dB vice the typical 0.01-0.03 dB loss for geometrically matched fibers. The Nufern fiber was then terminated with a connector having an eight (8) degree angle polish to avoid reflections and resulting damage due to back reflections being amplified as they traveled backwards through the gain fibers.

Alignment of the source beam with the connector was extremely difficult and resulted in less than a 50 % power insertion. In an effort to accurately estimate source power insertion into the Nufern fiber amplifier, a short (~1m) single mode fiber jumper with two manufactured 8 degree end polished connectors was used to measure maximum the coupled power insertion independently. The maximum power output of this jumper was measured and used as the coupled power efficiency for the remainder of the experiments.

With the known source input power, associated losses within the fiber, and the relationship between current and pump power, the first set of active fiber tests were conducted. Twenty meters of the Nufern fiber were carefully wound around a standard Corning insulated spool. Each fiber wind had a separation of at least two fiber diameters from the next nearest fiber wind in order to ensure thermal isolation. In this manner, the entire fiber length had a pump induced longitudinal temperature differential profile created from the thermal propagation within the core due to the nonradiative processes.

The experiment began by measuring the source output without the pump. The current driving the Alfalite pump was then activated. As the current was slowly increased, the output source power, current, residual pump power, and 4% of the output probe power were measured and recorded. Several plots were made to view the various relationships using conversions of current to input pump power.

After the insulated Nufern fiber test was completed, a new thermally conductive spool of similar dimensions was used to wind the twenty meters of fiber. The fibers were wound tightly together to ensure maximal thermal coupling. A conductive metallic sheet was placed on top of the wound fibers to further promote thermal equilibrium between fiber winds. Similar measurements were made, recorded and plotted as with the insulated fiber spool tests.

8.4 CASCADING ACTIVE YTTERBIUM-DOPED FIBERS VALIDATION EXPERIMENTAL SET-UP

For the cascading active fiber experiment, the input end of the Nufern fiber was cut back to ten meters. Ten meters of the 6.01 % Ge dopant fiber was then fusion spliced to the ten meters of 5.43% Ge dopant fiber. Since the geometries of both fibers were identical, the estimated loss in the fiber core due to the fusion splice was estimated to be 0.01 dB per splice. A connector with an eight degree angle polish was added to the end of the 6.01% Ge dopant fiber. Figure 23 depicts this order arrangement:
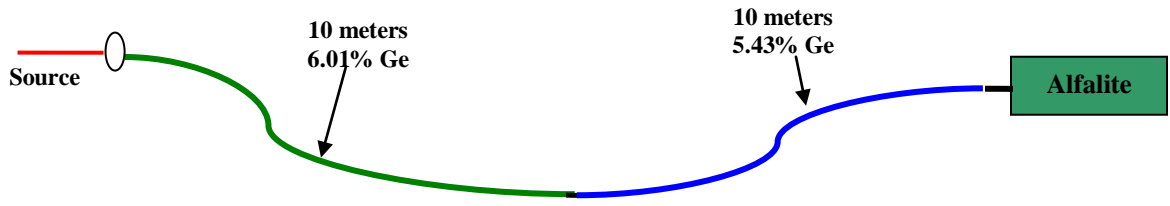
10 meters
6.01% Ge

10 meters
5.43% Ge

Source

Alfalite

Figure 23: Cascading fiber arrangement

This cascading arrangement was then wound around the insulating spool in the same manner described in section 8.3 to ensure thermal isolation between fibers. The same measurements described in section 8.3 were taken, recorded and plotted. Again, the cascading fiber arrangement was wound onto the conductive spool in the same manner as described in section 8.3 with the same data measured, recorded and plotted.

8.5 CASCADING ACTIVE FIBER STOKES FREQUENCY EXPERIMENTAL SET-UP

Although results from experiments described sections 8.3 and 8.4 provided a gross view of the dopant effects and temperature differentials, a more detailed evaluation of the effects on the Stokes peaks was required to determine the appropriate modifications and/or validation of the model. For this, the SBS probe set-up was required to measure the comprehensive effects of the cascading fibers on the various Stokes peaks as the probe varied its frequency across the range of responses. Figure 24 depicts this new arrangement:
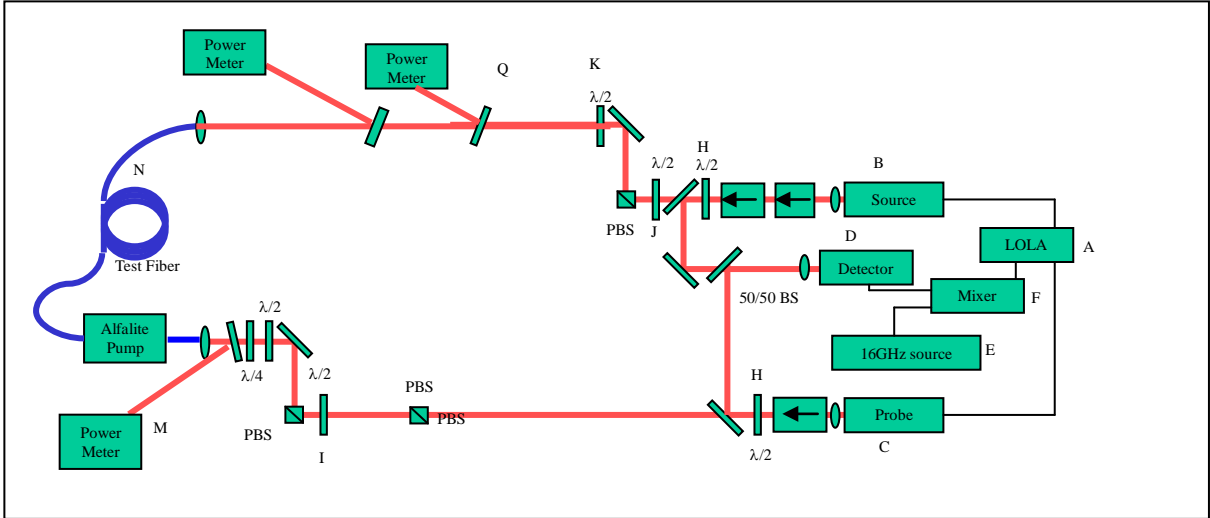
Figure 24: Cascading active fiber stokes response experimental set-up

In this set-up, the output source power is measured through a power meter (M) after being reflected by a 4% pick-off mirror in order to permit propagation of the probe. The probe and source polarizations were adjusted to provide maximal overlap within the fibers. The Alfalite pump and probe input powers were set to a value low enough to avoid threshold for each fiber segment.

The first set of experiments involved utilizing the insolated spool. Three probe sweep measurements were taken to observe both the locations and spread of each of the Stokes responses. This data was measured and recorded.

The second set of experiments utilized the conductive spool. Three similar sweeps of the probe were made with data being measured and recorded. In this manner, the temperature effects data could later be qualitatively de-coupled from the effects of increasing source power.

9   ACTIVE YTTERBIUM -DOPED FIBER RESULTS

9.1   SINGLE ACTIVE FIBER

The first important experimental result for all active fiber tests was determining the loss due to the fusion splice between the Alfalite pump and the dual clad fiber amplifier being evaluated. As stated previously, there was a mismatch of cladding diameters between the pump and the amplifier that resulted in a poor fusion splice after several attempts. The splice broke several times before I was able to initiate the experiments. The significant difference between the two cladding diameters was so dramatic that creating an appropriate recipe for the fusion took over three days.

As a result, there was a great deal of pump power loss at the fusion interface. Although the center core was aligned for acquiring sufficient data, the pump was not as fortunate. The splice became so hot during the experiments that it could not be touched.

After all experiments were completed, the active fiber was cleaved just after the splice to measure the coupled pump power into the active amplifier. Measurements of output pump power versus current drive for the Alfalite were measured and recorded for low pump powers. Next, the fusion splice was removed by cleaving the input pump fiber just before the splice. Again the output pump power versus the current drive for low pump powers were measured and recorded. The results are shown below:
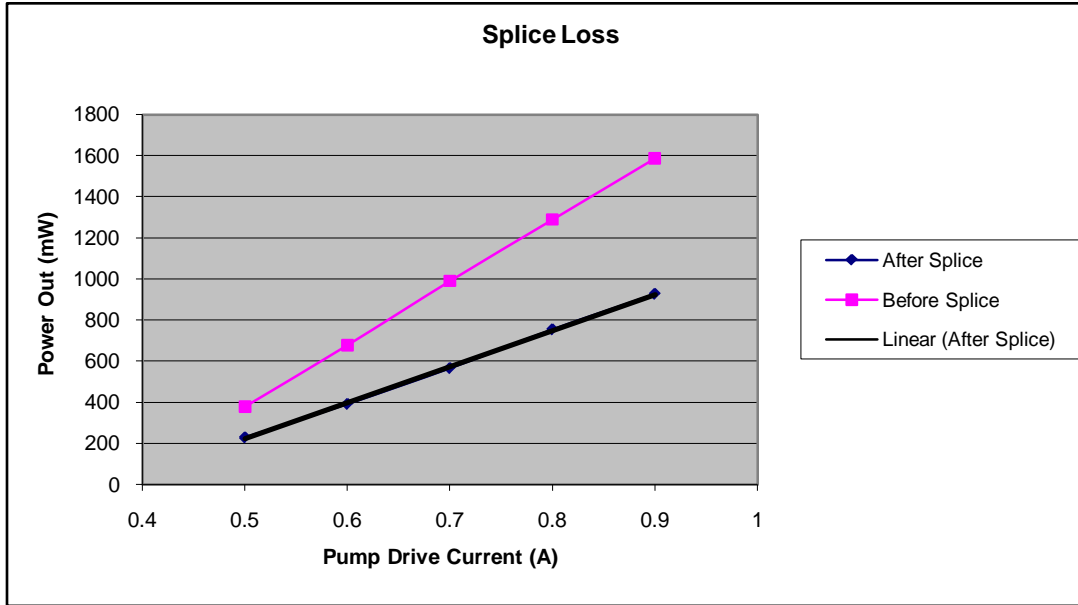
Figure 25: Fusion splice loss at pump/amplifier interface

The loss of power transfer due to the fusion splice was calculated to be ~42%. The associated relationship between the pump current drive and the coupled output pump power was calculated to fit a linear curve. This relationship was used throughout this chapter to provide accurate pump power values for the threshold measurements.

For twenty meters of 5.43 % Ge dual clad fiber amplifier, SBS threshold was assumed to be reached at ~3W of output signal where the Stokes power began to exceed 1% of the total output power value as shown below:
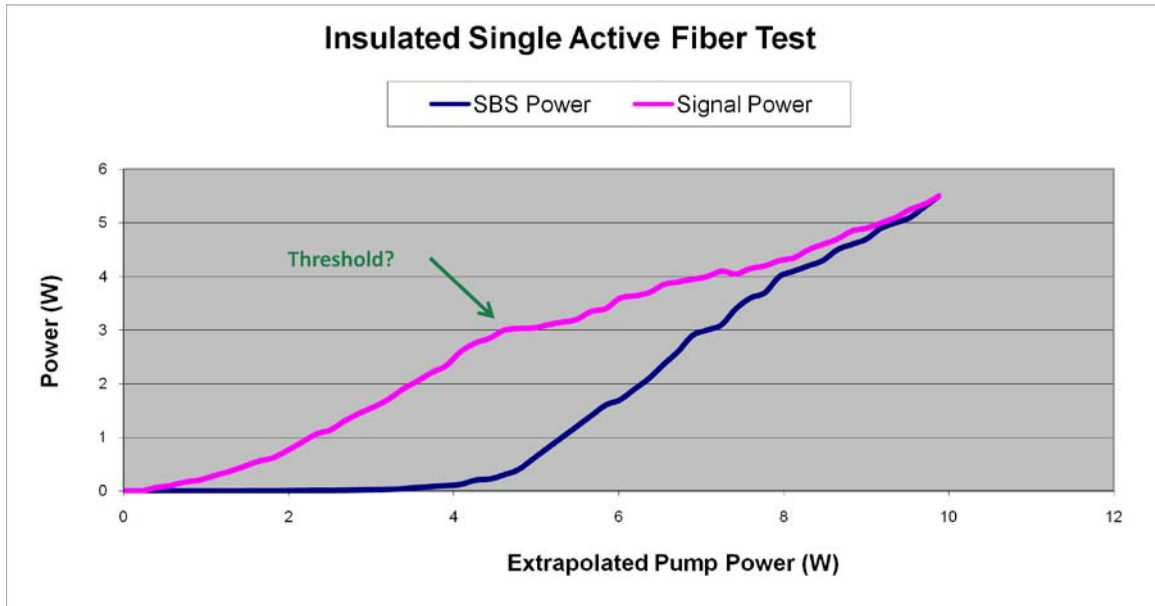

Figure 26: Active 5.43 % Ge single amplifier threshold-insulated spool

Although the total output power, both forward and backward, at 10W pump level appears to be 11W, this is merely a result of the uncertainty of measurement of the backward direction power. We have good certainty of the forward output power measured value due to our set-up, direct measurement method, and verified equipment calibrations. However, the backward measurement was not as accurate. It was an estimate based on a small percentage pick-off mirror and with not so well calibrated measurement system. It was only intended to provide a relative representation of the backward power to help identify the threshold point. As such, the appearance of a gain in total energy is the result of the uncertainty of measurement.

Although this particular experimental run demonstrates a near 3W threshold, other runs had thresholds ranging from 2.6W to 3.0W. For this reason we will use and average value of ~2.8W for our model adjustments. It must be noted that the pump power required for the ~3.0W threshold was only ~4.0W. This is in agreement with the claimed efficiencies by Nufern of 75%, as compared to 40% efficiencies for Er-Yb doped dual clad fiber amplifiers. For our model we need to know what fraction of the absorbed pump light contributed to heating in the fiber. In order to determine the contribution to heat generation within the core, it is necessary to subtract the residual pump power as shown below:

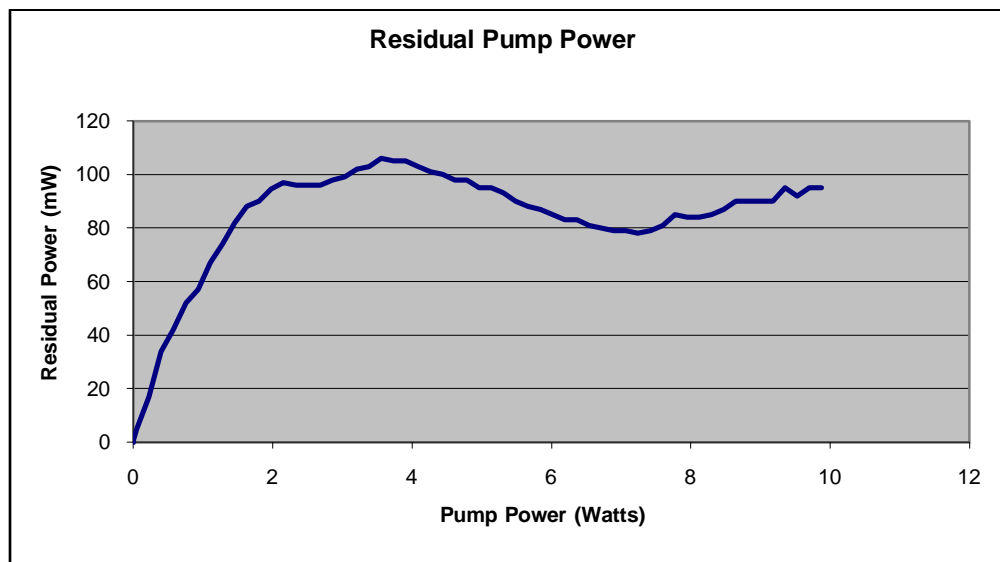**Figure 27: Residual pump power for 5.43 % Ge Single amplifier experiment**

From Figure 27, the residual pump power at threshold was only ~0.1W. In addition, at about 2.0W pump power, where the Stokes power began to absorb the pump more significantly, the residual pump began to reach a "threshold" of about 0.1 W. At this point, the total absorption within the fiber met the prediction of 95% for the 20 meter

segment. The decrease in the expected 5% residual pump power beyond the ~2.0W pump power was a result of the effects of the SBS gain within the core-as the SBS gain reached threshold, it too acquired gain from the ytterbium, thus causing additional pump depletion.

Evaluation of the residual power as shown in the figure above, it was determined that the continued increase in output power beyond threshold of ~3W was due to the contributions of higher even orders of SBS (2nd, 4th, etc). The change in the slope, as well as the bend, above 3W output, combined with continued intermediate bends and slope changes, were the accumulation of additional SBS higher even order powers.

Such multiple Stokes interactions can be understood as follows: The first Stokes wave in the backward direction now acts as a secondary signal source. As the power of the first Stokes wave increases, acoustic phonons created at the beginning of the amplifier now beat with the incoming Stokes signal creating a secondary Stokes interaction, downshifted ~16 GHz from the first. As the power of the secondary Stokes builds, the first Stokes reaches threshold. The secondary Stokes then builds, and the interaction with another odd order Stokes signal begins. The continued increase of output power in the forward and backward directions continues to build with increasing pump power as the various Stokes signals reach threshold and begin the process of higher order modes. The spectrum of the output power, however, will have various frequencies downshifted by two orders of Stokes, or ~ 32 GHz separation.

In order to verify this interaction above the ~3W threshold, a spectrum analyzer was used to evaluate the output. Data was observed at or near pump power levels of

about 9-10 W where it was assumed that several higher order Stokes waves were present. Figure 28 shows the observations directly taken from the spectrum analyzer:
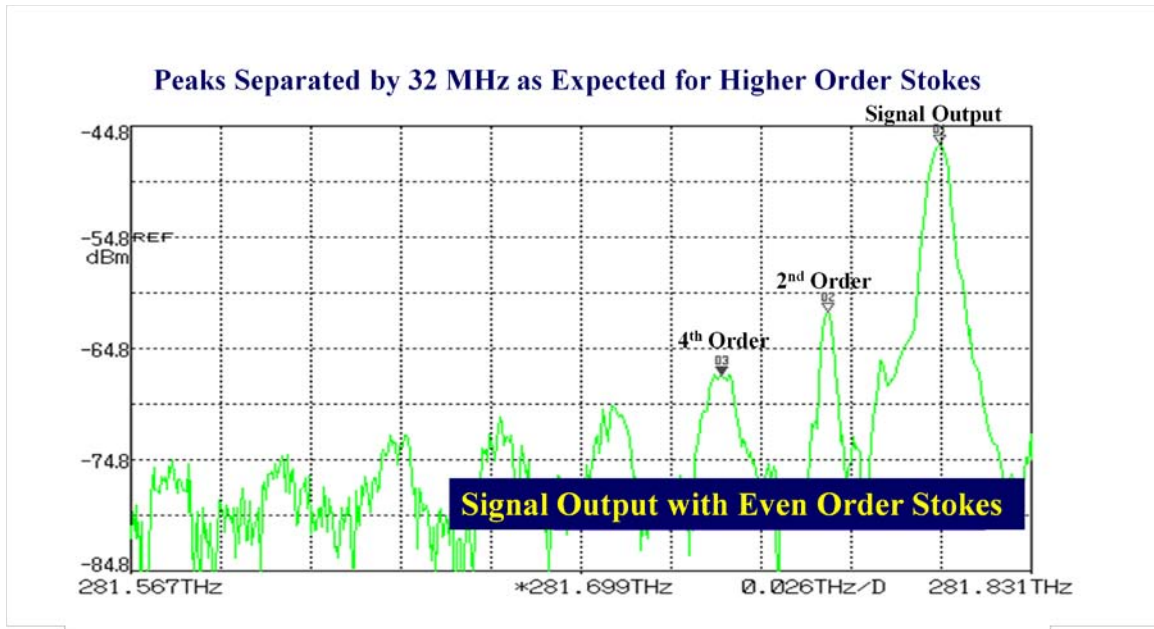

Peaks Separated by 32 MHz as Expected for Higher Order Stokes

Signal Output

2nd Order

4th Order

Signal Output with Even Order Stokes

Figure 28: Forward output spectrum of active amplifier with ~10W pump

The figure above clearly identifies several higher even order Stokes signals separated by the predicted 32 GHz. The first peak represents the original signal and the cascading peaks to the left represent the downshifted higher order even Stokes signals.

For completeness, spectrum measurements were taken near ~5W pump power levels to ensure the assumed threshold of ~3W was indeed the actual threshold. If there were no additional higher order Stokes waves immediately after the assumed threshold, then the estimated ~3W value would be validated. A scan of frequencies with a pump power near 3.5W yielded no findings of an additional Stokes wave. Therefore, we had reached our threshold at ~3W.

It was assumed that the multiple Stokes signals at higher power pump power levels would create Four-Wave mixing as described by Boyd[1]. Therefore, the pump

power was set to ~10W and another spectrum scan was conducted, this time including the higher frequencies predicted. Rather than the output location, the 4% reflected pick-off power was used just before the entrance of the signal into the fiber amplifier. The figure below shows the results of this scan:
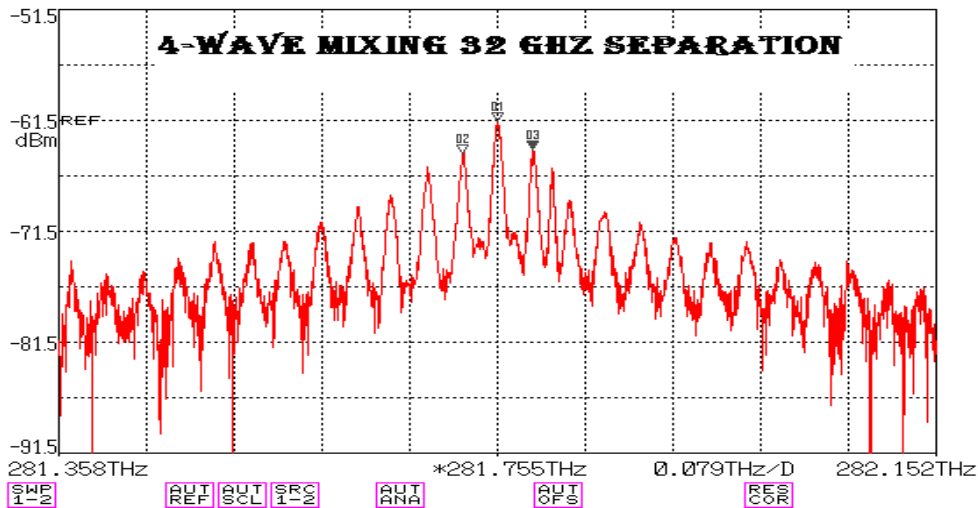

Figure 29: Four-wave mixing for single amplifier with ~10W pump power

From Figure 29, it is clear that Four-Wave mixing (FWM) was observed at this higher power levels. The mirrored, higher frequencies separated by 32 GHz, were typical for such FWM. A reflected signal separated by 16 GHZ was observed at the higher end of the frequency spectrum due to the fiber splice interface (< 1/60 reflection of the original signal) between the amplifier and the Alfalite fiber.

From the observations, additional power can be reached beyond threshold, increasing somewhat linearly with the pump power. Actually, there are many fiber laser manufacturers that reach higher levels of power, including IPG, by exceeding the SBS

threshold. However, the power increased beyond the SBS threshold is not beneficial for coherent Beam Combining applications due to the independent frequencies separated by 32 GHz.

9.2 SINGLE ACTIVE FIBER WITHOUT THERMAL DIFFERENTIAL

As described in section 8.3, a specially designed aluminum spool containing groves for the fiber to be wound within, cooled with circulating water, was utilized to remove the thermal gradient along the fiber length as a result of the nonradiative processes from the pump-ytterbium interaction. In essence, the exceptional conductivity of aluminum coupled with the circulation of the cooled water increased the value of "h", or convection coefficient at the surface of the fiber. It was hoped that this approach would remove the majority of temperature differential along the fiber in order to provide a non-thermal gradient baseline for model comparison and adjustment.

The aluminum spool utilized was hollow inside so that cooled water could pass through it. The circulated water was cooled to a constant 17.5 C. As the pump current source was increased, the output, Stokes, and residual pump powers were measured and recorded for several runs. Each of the runs resulted in a various values for the threshold ranging from 1.4 to 1.7 W. The average pump power required to reach threshold was over 2 W. Output power threshold was verified with reflected SBS power and residual pump powers similar to the method described in section 9.1. Specifically, threshold reached is when SBS power to output power exceeds 1% and when the residual pump power begins to reach a threshold. The result for one of the experimental runs is displayed below:
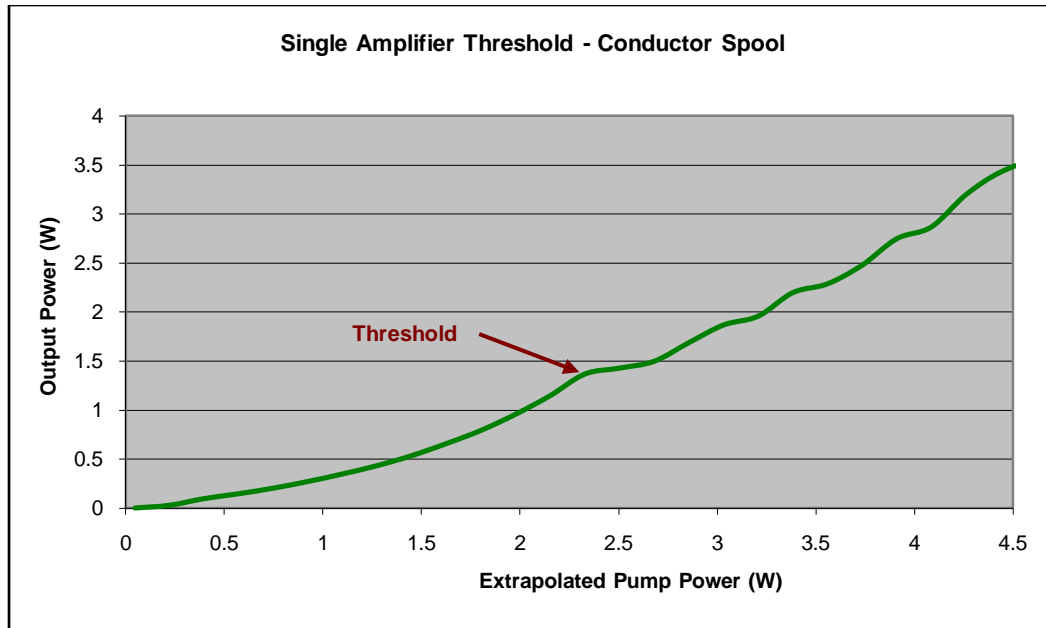
Figure 30: Active amplifier threshold – conductor spool

It appeared that the output power began to "clamp" around 1.4W, or ~3dB less

than the previous experiment which permitted the full temperature gradient by utilizing

the insulator spool. Taking all the data sets into account, the average threshold to be used

for the model will be ~1.6 W. As in section 8.1, an optical spectrum analyzer was used to

verify that the continued increase in output power beyond threshold was due to increasing

powers of even order Stokes.

Based on the estimates from the model, the increase in threshold power should

have been significantly smaller. The significant increase in SBS threshold for the

insulator spools suggests, as stated earlier, that our "h" value and associated thermal

model requires adjustment for this significant thermal differential witnessed from actual

experiments. Such adjustments and considerations are made in chapter 9.

9.3 CASCADING ACTIVE FIBER

Similar to the single 5.43 % Ge concentration by weight ytterbium doped dual clad fiber amplifier experiments in sections 9.1 and 9.2, both thermal gradient and constant core temperature experiments were conducted for both cascading fiber amplifiers. The arrangement desired was described in section 8.4 with the pump fiber fused to ten meters of 5.43 % Ge fiber fused to ten meters of 6.01% Ge fiber with an 8° angle polished connector.

The first experiment evaluated the cascading fibers with a significantly mitigated thermal gradient by once again utilizing the conductive aluminum spool cooled to 17.5 ^{o}C. The results are shown in Figure 31:

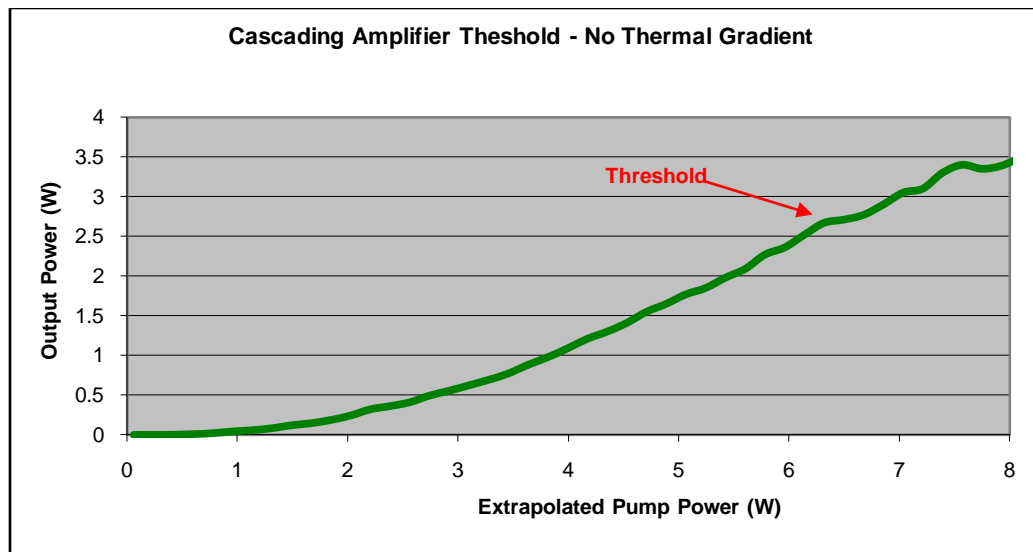**Figure 31: Cascading active fiber threshold – conductor spool**

The average threshold for the measurements taken was ~2.7W. The increase without a thermal gradient was ~1.7 times that of a single fiber amplifier. This is what we might expect for two equal lengths of passive fiber segments, thus consistent with an assumption that we removed any measureable effects of a thermal gradient along the

length of the fiber. Further analysis of the Stokes response in section 9.4 will provide clarification as to the difference in model expectations to the results.

The same threshold experiment was conducted utilizing the same insulator spool in section 9.2. The results are shown below:
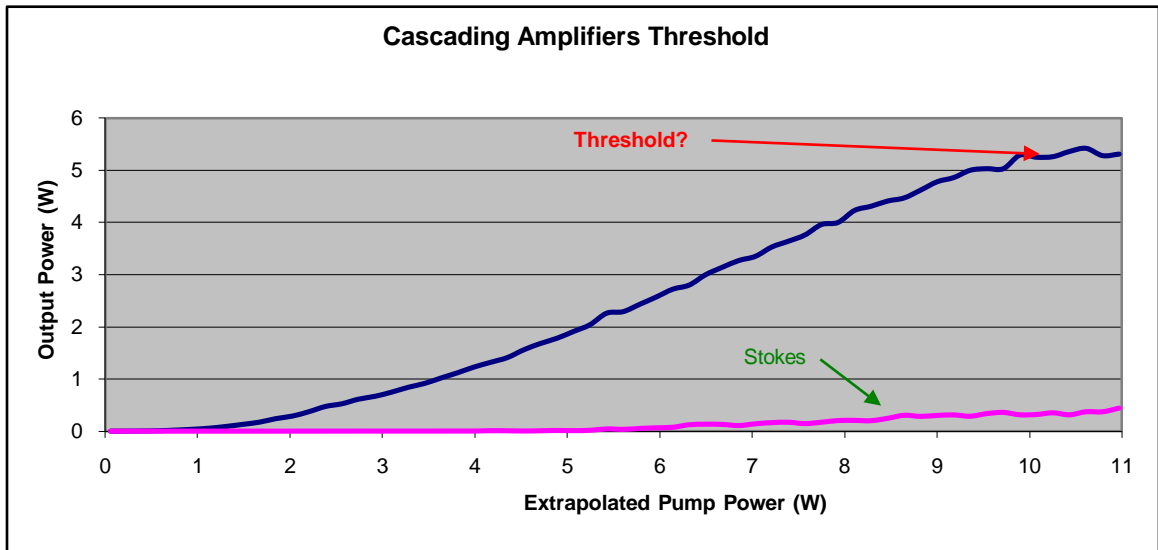
Figure 32: Cascading amplifiers threshold

From the results, it appears that the threshold is ~5.4W. Interestingly, the SBS power does not appear to be dominating at this value. To be confident in the measurement, one would require greater pump power and observation of the Stokes power. For now, however, we will assume this is our threshold. In comparison with the mitigated thermal gradient cascading amplifiers, there is an increase in output power by a factor of two. This is significant considering our model only predicted a slight increase due to a few degrees of temperature gradient along the fiber. Before any adjustments are made to the model, an evaluation of the Stokes response with and without the thermal

gradient should be made. In addition, each fiber type should be evaluated at low pump powers to determine the individual center frequencies and associated linewidths.

9.4   ACTIVE FIBER STOKES PEAK AND LINEWIDTH RESPONSE

The final measurements for this dissertation utilized the novel SBS probe arrangement and technique described in the set-up portions of this dissertation. By measuring and analyzing the center frequencies and linewidths of the individual fiber amplifiers, as well as the combined cascading amplifier configuration for both thermal gradient and somewhat constant core temperatures, it was hoped to acquire enough information to adjust the model appropriately. Although it was predicted that a linewidth of 40 MHz was accurate, physical material properties and processing methods would cause unique deviations. In addition, such measurements would also provide adjustments to the required % Ge by weight concentrations that would be required to shift the Brillouin center frequency by a linewidth. Only empirical results would provide the necessary adaptations to the model to be an effective predictive tool.

The results were first acquired for the cascading fiber arrangement and then for the individual fibers. However, in order to present in a more logical process, the individual fiber amplifier profiles will be presented first. In addition, three revelations will be revealed as to why there were significant discrepancies in our predictions from the results in sections 9.1-9.3.

The Stokes probe was conducted for each of the two fibers having 20 meter lengths using a relatively low pump power of ~0.6W to avoid significant spread of the linewidth due to any thermal gradients. In addition, an associated Lorentzian line shape, slightly smaller (to account for any thermal spread) than the SBS profile spread, was fit to

the data for comparison. Several measurements were taken yielding consistent results. The actual data points for one such typical measurement are blue dots while the Lorentzian is a solid red line. The figure below shows such data for the 6.01 % Ge dual clad ytterbium doped fiber amplifier:

Figure 33: 6.01 % Ge active fiber – conductor spool

The Lorentzian was an excellent fit to the data as expected, with a center frequency of 15.827 GHz and a linewidth 55 MHz. Recall that we used a Lorentzian linewidth of 40 MHz for our model based on the passive data experiments.

Several measurements were also taken for the 5.43 % Ge fiber wound around the cooled conductor spool. Again, the actual data points for one such typical measurement are blue dots while the Lorentzian is a solid red line. The figure below shows such data for the 5.43 % Ge dual clad ytterbium doped fiber amplifier:
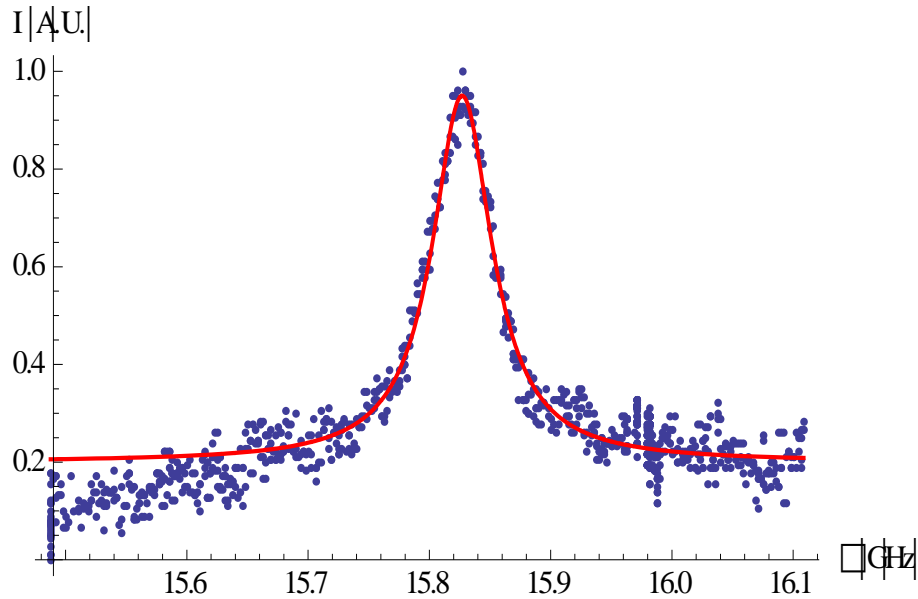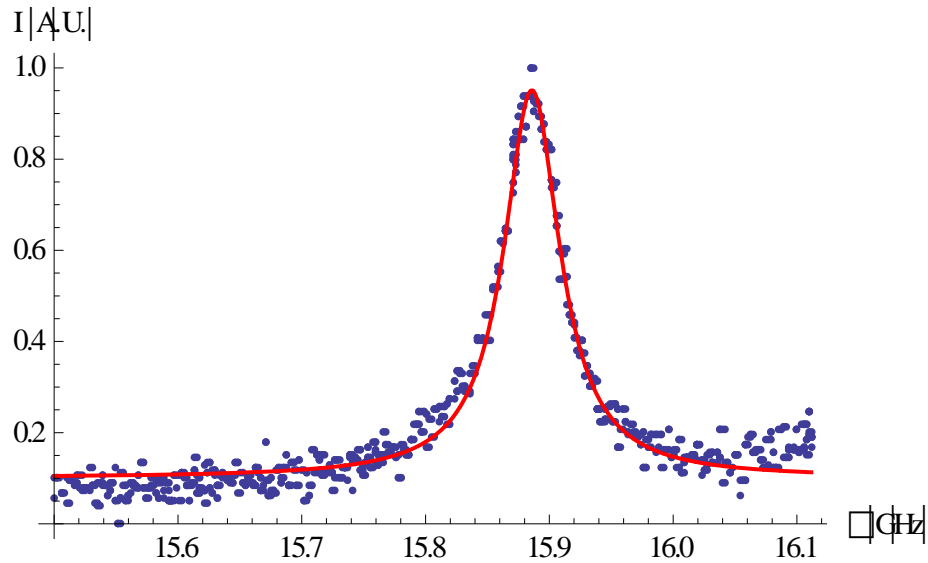
Figure 34: 5.43 % Ge active fiber – conductor spool

Although the Lorentzian linewidth of 55 MHz was the same for the two fibers, the center frequency was 49 MHz greater with a measurement of 15.882 GHz. Our passive fiber measurements predicted an 89.15 MHz/% Ge. From the passive fiber results, we should have observed a downshifted frequency of 51.7 MHz, or center frequency of 15.830, very close to the actual value of 15.827. For future model development, we will use our active fiber results of 94.83 MHz/%Ge rather than the value of 89.15 MHz/%Ge obtained from our passive fiber results. The significance of these results is that our estimate of ½ % Ge concentration between active fiber segments is a good approximation to ensure separation of the effects of Stokes wave on preceding fiber segments.

The two segment cascading fiber configuration, each segment being 10 meters in length, was wound on the aluminum conducting and cooled spool. Similar measurements were taken as those for the individual fibers. The results are shown below:

94
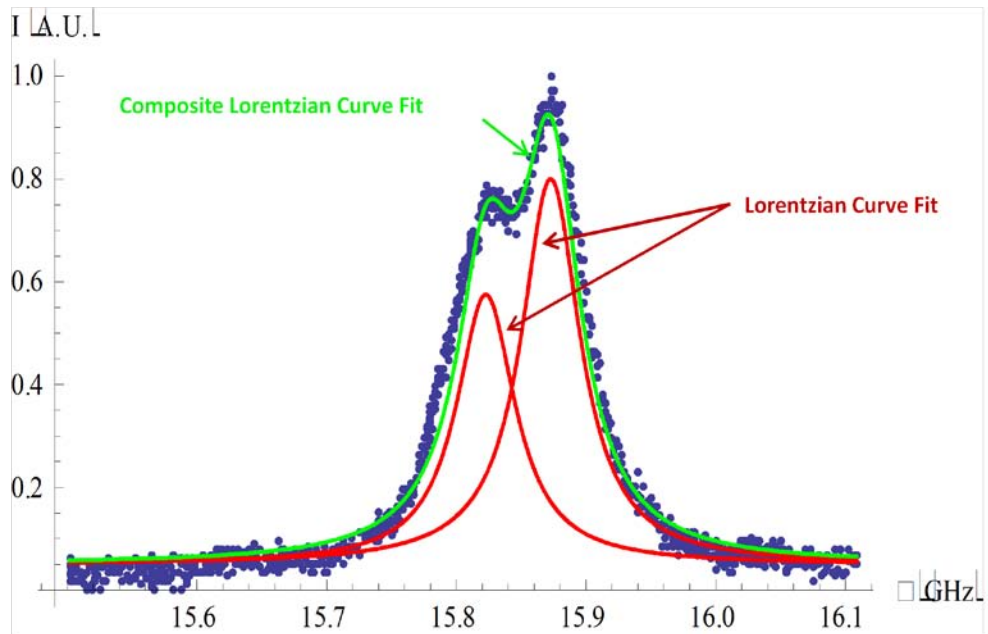
Figure 35: Cascading active fibers – conductor spool

As expected, only two peaks were observed. The separation between the two peaks was about 50 MHz with a linewidth of 55 MHz for each segment as expected. The fiber closest to the pump (5.43 % Ge) had a significant peak compared to the one farthest away. The increased power of the signal nearer to the pump produced a stronger response to the SBS signal, thus a higher peak for that fiber segment region. Hopefully, there will be enough thermal gradient to compensate for the increased signal power effect at the 5.43 % Ge segment.

Below are the results for the cascaded amplifier with a thermal gradient:
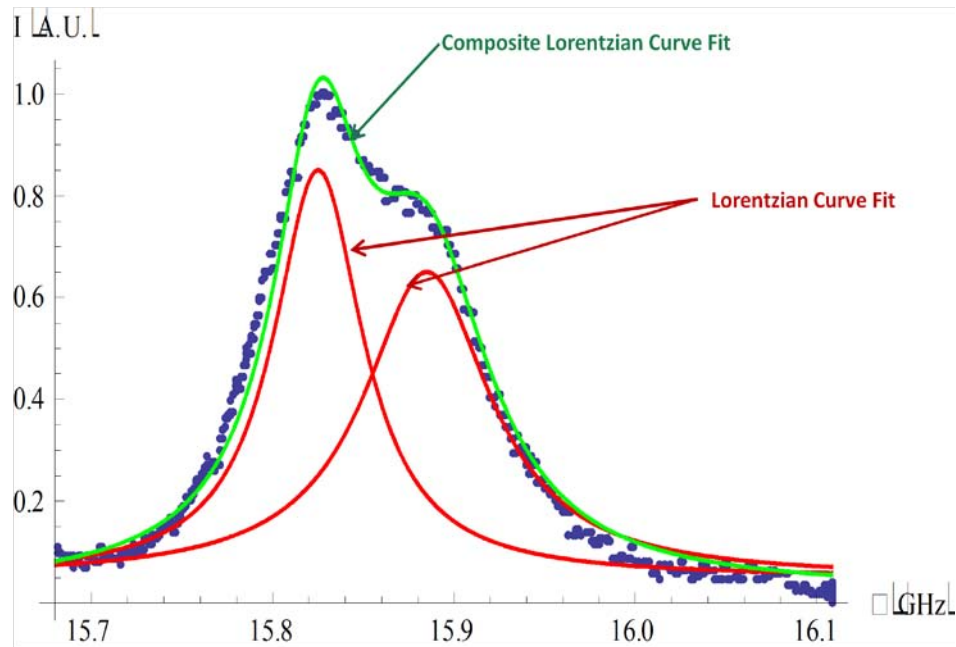
Figure 36: Cascading active fibers – with thermal gradient

With the thermal gradient, there are several noticeable attributes. First, the peak

of the 5.43 % Ge is now significantly lower than the 6.01 % Ge peak. In addition, the

frequency separation is now 60 MHz rather than 50 MHz. Finally, the Lorentzian

linewidth for the 5.43 % Ge is 85 MHz while the 6.01 % Ge is 60 MHz. The spread from

55 MHz to 85 MHz for the 5.43 % Ge indicates a significant temperature differential

within the length of the fiber segment. In addition, the increase in the linewidth of the

6.01 % Ge indicates additional temperature change in this region, although much smaller

than the first segment. The 10 MHz increase in center frequency separation represents an

integrated SBS response due to the temperature differential.

All this together indicate a significant temperature differential along the fiber

length not predicted by our initial assumptions for our model. This information also

compliments and agrees with the threshold values found in sections 9.1-9.3, where the thermal gradient increased the threshold by a factor of two.

An explanation for this discrepancy can be presented through the second revelation. The fibers had two significant aspects that were not included in the initial model. First, the second cladding was made of a material unlike the first. This material was an ultraviolet curing durable acrylate with thermal conductivity less than 0.1 that of typical silica for the first cladding. The diameter was ~350 um-an additional 75um radius from the first cladding. This alone provides additional temperature differential within the core. Second, the fiber was wrapped around a plastic spool surrounded by excellent insulating foam. The pressure of the tightly wound fiber created an insulation barrier around ~60% of the fiber. Since the heat could not escape on this region it significantly reduced the "h" value of that for a fiber suspended in air. The figures below are diagrams illustrating these two contribution conditions:
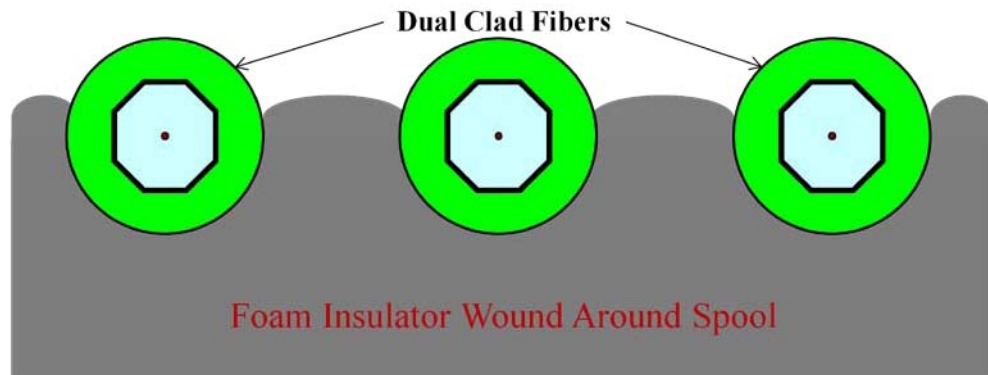

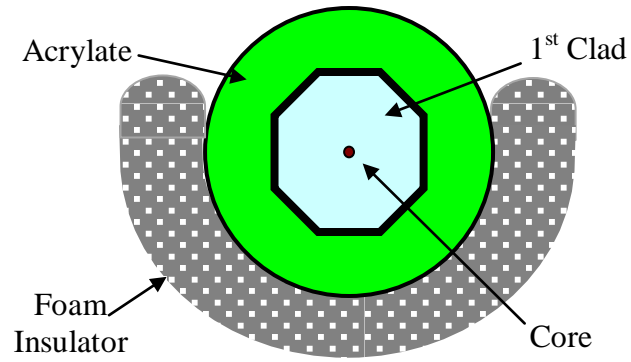**Figure 37: Dual clad fibers wrapped around insulator spool**

Figure 38: Dual clad fiber in insulator

These two additional effects contributed to the significant increase in temperature

differentials along the fiber length not predicted with initial estimates.

10   COMPARISON WITH MODEL AND ADJUSTMENTS

From the results of the active fiber experiments presented in chapters 5 and 9, the most significant changes to our overall model are in the prediction of the temperature gradient within the core and the adjustments to the Brillouin linewidths for the active fibers used. For the later, the model will utilize ~55 MHz linewidths. In addition, the fiber segments will be separated by 0.5% Ge by weight to ensure limited interaction between segments of the Brillouin frequencies. For the former, the "h" value for surface convection will be reduced (by 60%) to 0.4 W/m^2 to account for the insulator around the spool. Adjusting the model to more accurately account for the geometry of the fiber and associated convection coefficients is required. Recall the original assumed that the claddings could be assumed as a single region, described by the equation below:

$$\Delta T(z) = \left(\frac{\alpha \eta a^2}{\pi b^2 4k} \right) \left[1 + 2\ln\left(\frac{c_{clad}}{a} \right) + \frac{2k}{c_{clad}h} \right] P_p(z). \tag{63}$$

We change this model to account for the less than 0.1 conductivity of silica for the 2nd cladding, as well as adding an adjustment factor "Z". The Z-coefficient is used to account for the additional localized heating of the fiber core as a result of the temperature build-up resulting from the insulator blocking heat transfer. The longitudinal temperature distribution equation now becomes:

$$\Delta T(z) = Z \left(\frac{\alpha \eta a^2}{\pi b^2 4k} \right) \left[1 + 2\ln\left(\frac{b}{a} \right) + 20\ln\left(\frac{d}{b} \right) + \frac{20k}{dh} \right] P_p(z), \tag{64}$$

where d is the diameter of the 2nd cladding.

Note: $k_{plastic}$ = 10x k_{glass} (we use 20k instead of 2k).

In an attempt to match the SBS linewidth of the model to the experimental results for the thermal, an initial estimate of "Z" was set at "1.0/(1.0-fraction of insulated cladding)", or "1.0/0.4". With these changes, our model was able to predict the linewidth results presented in chapter 8 for the two fiber segments within the cascaded fiber arrangement. The model results with these modifications for the fiber segment with the greatest thermal differential (5.43 % Ge)-the segment next to the counter-pumped source-are shown below:
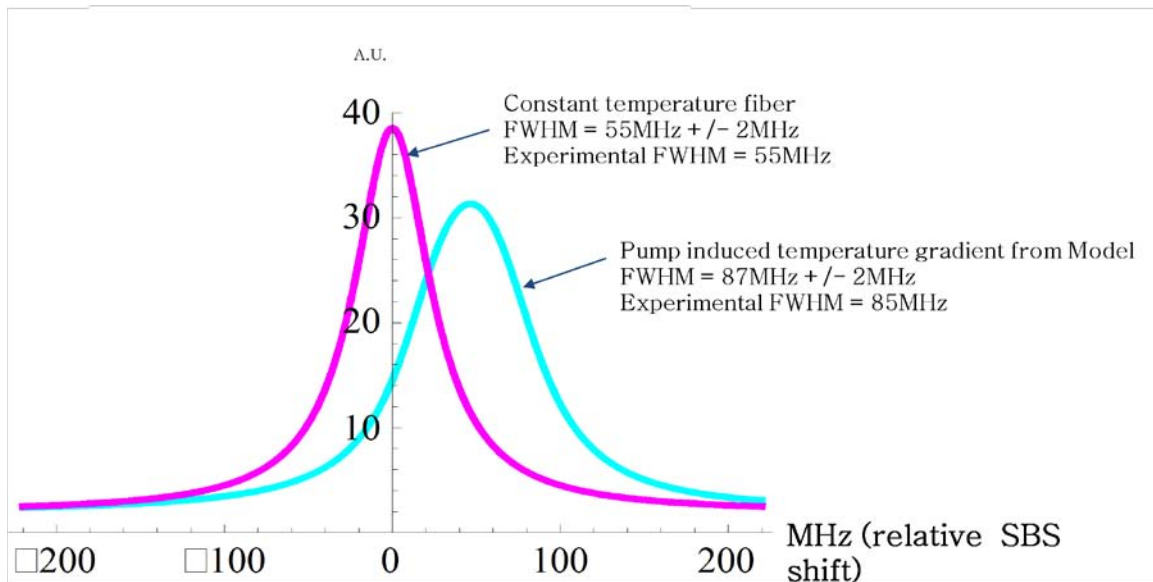

Figure 39: Model prediction of SBS gain spectrum for 5.43 % Ge fiber segment - with and without thermal gradient

11 CONCLUSIONS

11.1 SYNOPSIS OF RESULTS

A theoretical model has been developed to mitigate the SBS threshold for fusion spliced fiber segments of varying % Ge by weight. The model was developed in an iterative process, first utilizing passive fiber results and then moving on to the more complicated active fiber results. Empirical data baseline the model and provided substantial insight into the physics in order to further adjust the model.

The most significant finding was the change in the thermal gradient along the fiber length. Initial model predictions only indicated a few degrees change, while experimental data indicated differentials in double digits. The use of an acrylate 2nd cladding and an insulator between the fiber and spool added a dramatic contribution to the temperature differential within the core along the propagation length.

Experimental data of active ytterbium-doped dual clad fiber amplifiers have demonstrated that sequential fiber segments should be separated by ½ % Ge by weight. The cascaded system must be counter pumped with increasing % Ge by weight segments starting at the pump end. The fiber exiting the pump needs to be matched to the numerical aperture and physical dimensions of the first amplifier to ensure efficient coupling of the pump power. Due to the limitation of fusion splicing, the smaller fiber segment length should not be below 20 cm.

Assuming the maturity of fiber manufacturer by 2010, it is estimated that an increase in both diameters of the core and ytterbium dopant concentrations are possible. It has been estimated that with these considerations, the SBS threshold can be increased by a factor of 20 from the values we experienced. This means that without the cascaded

fibers, using standard manufacturing, with a few advances, we could achieve a narrow line, single mode power output of nearly 40W.

The active fiber amplifier tests have demonstrated the ability to increase SBS by a factor of two for each fiber segment. The follow is a summary of our test results:

	Conductor Spool	Insulator Spool	Increase Factor
One Single Fiber	1.4W	3W	~2x
Two Cascading Fibers	2.7W	5.4W	~2x
Increase Factor	~2x	~2x	~4x

Figure 40: Active fiber amplifier summary results

The results have shown that, if fiber lengths are chosen to match the overall SBS effects of the thermal gradient, we can provide an extremely valuable design tool from our model to create a high power narrow linewidth fiber amplifier from several segments made of varying % Ge concentration cores.

Now, if we assume the ability for the manufacturer to provide a range of Ge concentrations within the core of nearly10%, twenty fiber segments could be combined utilizing our theoretical model to determine the appropriate length of each fiber. Providing we can maximize each fiber length's effectiveness for the temperature differential and coupled power effects, we will have an estimated forty fold increase in output power. The potential power output of a single cascaded fiber amplifier for utilizing standard dual clad fiber amplifier manufacturing capabilities would be ~1.6 kW without SBS! This potential benefit, however, is constrained by the limitations presented

in this dissertation. Perhaps a more conservative approach would be to use 12 fiber

segments resulting in an overall single fiber output ~1kW.

11.2   BENEFITS

The most significant benefits of this dissertation is the utilization of intrinsic

thermal differential properties within the fiber core as well as the ability to manufacture

inexpensive fiber amplifiers utilizing common fabrication and standard equipment to

provide low cost solutions. In addition, the model developed within this dissertation can

be utilized as a predictive tool to avoid unnecessary experimental costs and associated

time for developing an SBS mitigated narrow linewidth fiber amplifier. Finally, the use

of inexpensive cascaded fiber, produced in a short period of time with great accuracy and

reliability, having a narrow linewidth output, enables an effective and efficient

demonstration of high power coherent beam combining of dozens of fibers for a variety

of industrial and government applications. This in turn will provide the validation

necessary for continued research and eventual deployment of high power tactical and

strategic fiber lasers for the defense of our nation.

11.3   LIMITATIONS

Although this work has provided a positive potential for the growth of high power

fiber lasers, there are several limitations. The first is the ability of manufacturers to

maintain constant density within the fiber core of all the other key elements while

changing the % Ge by weight and maintaining a constant index of refraction within the

core.

In addition, fusion splicing of several fiber segments may introduce issues with

maintaining a center threshold for coherence lengths required for coherent beam

combining. Each splice will introduce an additional loss of coherence. The sum of nearly 20 segments may exceed the required constraints placed on this technology. Also, there may be issues at higher temperatures and power levels for fusion splices.

The time and ability to ensure quality fusion splices is also an issue. There will need to be a repeatable method utilized in order to ensure consistency. In addition, the time to splice must be minimized to ensure low cost production.

The ability to accurately predict the thermal gradient within the fiber core for these fibers will also constrain the potential output power of this approach. Although this dissertation provided an initial thermal model, adaptations were required based on empirical results. A more robust thermal model will be required to account for the unique configurations to be used.

Finally, the solubility of ytterbium must be maintained for the varying increases in % Ge. It is still uncertain the effects of such high concentrations of % Ge on ytterbium solubility. Further experiments and challenges to the manufacturing capabilities are required.

11.4   FUTURE WORK-NEXT STEPS

In order to fully exploit these findings and model presented in this dissertation, several future activities and experiments should be explored. First, the maximum core diameter for single mode with a numerical aperture of ~0.06 should be ordered. These fibers should span the estimated 10% Ge differential with the highest level of ytterbium concentration possible. At least ten fibers should be purchased, differing by 1.0% Ge by weight. Verification of the results performed in this dissertation should be performed. Once the verification is made, the individual fiber results should be utilized with the

model in order to predict the appropriate fiber lengths. These should be cascaded and evaluated.

Included in the first work mentioned above, should be high power pumps near 2.0 kW to reach the desired threshold for each cascaded fiber configuration. This experiment in itself will determine any additional limitations to the model and approach.

As mentioned, the ability to coherently beam combine these fusion spliced fiber must be evaluated. Starting with low power of several cascaded fibers, one could gradually build up in power and numbers. The gradual addition of both complexity and numbers will enable the overall determination of whether or not this approach will have utility for coherent beam combining.

Finally, an extensive development of a more robust thermal model must be explored to account for the various fiber material, geometries, and configurations to be used. Analysis and observation of the temperature within the core should be sought to ensure an accurate temperature profile along the core is obtainable.

REFERENCES

1.   Boyd, R.W., *Nonlinear Optics*. 1992, Boston: Academic Press, Inc. 439.

2.   Agrawal, G.P., *Nonlinear Fiber Optics*. 3 ed. 2001, San Diego: Academic Press, Inc. 466.

3.   Lichtman, E., R.G. Waarts, and A.A. Friesem, *Stimulated Brillouin scattering excited by a modulated pump wave in single-mode fibers.* Journal of Lightwave Technology, 1989. **7**(1): p. 171-174.

4.   Chraplyvy, A.R., *Limitations on Lightwave Communications Imposed by Optical-Fiber Nonlinearities.* Journal of Lightwave Technology, 1990. **8**(10): p. 1548-1557.

5.   Conentino, A. and E. Iannone, *Threshold dependence on line coding In phase-modulated coherent optical systems.* Electronics Letters, 1989. **25**(21): p. 1459-1460.

6.   Kim, N.S., *Numerical analysis and experimental results of output performance for Nd-doped double clad fiber laser.* Optical Communications, 2000. **180**: p. 329-373.

7.   Imai, Y. and N. Shimada, *Dependence of Stimulated Brillouin Scattering on Temperature Distribution in Polarization-Maintaining Fibers.* IEEE Photonics Technology Letters, 1993. **5**(11): p. 1335-1337.

8.   Canat, G., et al., *Characteristics of the Brillouin spectra in erbium-ytterbium fibers.* Optics Express, 2008. **16**(5): p. 3212-3222.

9.   Kovalev, V.I. and R.G. Harrisson, *Analytic modeling of Brillouin gain in rare-earth doped fiber amplifiers with high-power single-frequency signals.* Proc. of SPIE, 2005. **5709**: p. 142-146.

10.   Jeong, Y., J. Nilsson, and J.K. Sahu, *Single-frequency, polarized ytterbium-doped fiber MOPA source with 264 W output power*, in *Conference on Lasers and Electro-Optics*. 2004. p. 1065-1066.

11.   Koyamada, Y., et al., *Simulating and designing Brillouin gain spectrum in single mode fibers.* Journal of Lightwave Technology, 2004. **22**: p. 631-639.

12.   Shiraki, K., M. Ohashi, and M. Tateda, *SBS threshold of a fiber with a Brillouin frequency shift distribution.* Journal of Lightwave Technology, 1996. **14**: p. 50-57.

13.   Kurashima, T., T. Horiguchi, and M. Tateda, *Thermal effects of Brillouin gain spectra in single-mode fibers.* IEEE Photonics Technology Letters, 1990. **2**: p. 718-720.

14.   Kuzin, E.A., M.P. Petrov, and A.A. Fotiadi, *Fiber-optic stimulated-Brillouin-scattering amplifier.* Soviet Physics Technical Physics, 1988. **33**(2): p. 206-209.

15.   Kim, H.S., et al., *Threshold reduction of stimulated Brillouin scattering by the enhanced Stokes noise initiation.* Applied Physics Letters, 1999. **74**(10): p. 1358-1360.

16.   Culverhouse, D., et al., *Potential of stimulated Brillouin scattering as sensing mechanism for distributed temperature sensors.* Electronics Letters, 1989. **25**: p. 913-914.

17.   Cotter, D., *Suppression of stimulated Brillouin scattering during transmission of high-power narrowband laser light in monomode fibre.* Electronics Letters, 1982. **18**(15): p. 638-640.

18.   Liu, A., *Suppressing stimulated Brillouin scattering in fiber amplifiers using nonuniform fiber and temperature gradient.* Optics Express, 2007. **15**(3): p. 977-984.

19.   Smith, R.G., *Optical Power Handling Capacity of Low Loss Optical Fibers as Determined by Stimulated Raman and Brillouin Scattering.* Applied Optics, 1972. **11**(11): p. 2489-2494.

20.   Shiraishi, K., Y. Aizawa, and S. Kawakami, *Beam expanding fiber using thermal diffusion of the dopant.* Journal of Lightwave Technology, 1990. **8**: p. 1151-1161.

21.   Lee, C.C., P.W. Chiang, and S. Chi, *Utilization of a dispersion-shifted fiber for simultaneous measurement of distributed strain and temperature through Brillouin frequency shift.* IEEE Photonics Technology Letters, 2001. **13**: p. 1094-1096.

22.   Le Floch, S., F. Riou, and P. Cambon, *Experimental and theoretical study of the Brillouin linewidth and frequency at low temperature in standard single-mode optical fibers.* J. Opt. A.; Pure Appl. Optics, 2001. **3**: p. L12-L15.

23.   Shiraki, K., M. Ohashi, and M. Tateda, *Suppression of stimulated Brillouin scattering in a fiber by changing the core radius.* Electronics Letters, 1995. **31**: p. 668-669.

24.   Wang, Y., C.-Q. Xu, and H. Po, *Thermal effects in kilowatt fiber lasers.* IEEE Photonics Technology Letters, 2004. **16**: p. 63-65.

25. de Oliveira, C.A.S., et al., *Stimulated Brillouin scattering in cascaded fibers of different Brillouin frequency shifts.* Journal of Optical Society of America, 1993. **10**: p. 969-972.

26. Buckland, E.L. and R.W. Boyd, *Measurement of the frequency response of the electrostrictive nonlinearity in optical fibers.* Optics Letters, 1997. **22**(10): p. 676-678.

27. Bolle, A., G. Grosso, and B. Daino, *Brillouin gain curve dependence on frequency spectrum of PSK-modulated signals.* Electronics Letters, 1989. **25**(1): p. 2-3.

28. Hadjifotiou, A. and G.A. Hill, *Suppression of stimulated Brillouin backscattering by PSK modulation for highpower optical transmission.* IEEE Proc. J, 1986. **133**: p. 256-258.

29. Jeong, Y., et al., *Power scaling of single-frequency ytterbium-doped fiber master oscillator power amplifier sources up to 500 W.* IEEE J. of Selected Topics in Quantum Electron, 2007. **13**: p. 546-551.

30. Broderick, N.G.R., Offerhaus, H. L., Richardson, D. J., Sammut, R. A., Caplen, J. and Dong L., *Large mode area fibers for high power applications.* Optical Fiber Technology, 1999. **5**: p. 185-196.

31. Ji Wang, S.G., Donnell Walton, Ming-Jun Li, Xin Chen, A. Boh Ruffin, Jeffrey Demeritt, and Luis Zenteno, *High performance Yb-doped double-clad optical fibers for high-power, narrow-linewidth fiber laser applications.* Proceedings of SPIE 2006. **6351**(635109-1).

32. Ming-Jun Li, X.C., Ji Wang, Stuart Gray, Anping Liu, Jeffrey A. Demeritt, A. B. Ruffin, Alana M. Crowley, Donnell T. Walton, and Luis A. Zenteno *Al/Ge co-doped large mode area fiber with high SBS threshold.* Optics Express, 2007. **15**(13): p. 8290-8299.

33. Dragic, P.D., et al., *Optical fiber with an acoustic guiding layer for stimulated Brillouin scattering suppression.* CLEO, 2005. **3**: p. 1984-1986.

34. Mermelstein, M.D., et al., *11.2 dB SBS gain suppression in a large mode area Yb-doped optical fiber.* Proc. of SPIE, 2008. **6873**: p. 68730N-68730N-7.

35. Tetsuya Nakanishi, M.T., Takemi Hasegawa, Masaaki Hirano, Toshiaki Okuno, and Masashi Onishi, *Al2O3-SiO2 Core Highly Nonlinear Dispersion-shifted Fiber with Brillouin Gain Suppression Improved by 6.1dB.* ECOC, 2006. **PDP**: p. Th4.2.2.

36.   Nilsson, J., et al., *SBS Suppression at the kW Level*, in *Photonics West*. 2009: San Jose, CA.

37.   Gapontsev, D. *6kW CW Single Mode Ytterbium Fiber Laser in All-Fiber Format*. in *Solid State and Diode Laser Technology Review*. 2008. Albuquerque, NM: Directed Energy Professional Society.

38.   Li, M.-J., et al., *Fiber designs for higher power lasers.* Proceedings of SPIE, the International Society for Optical Engineering, 2007. **6469**: p. 64690H.1-64690H.9.

39.   Fini, J.M., *Bend-resistant design of conventional and microstructure fibers with very large mode area.* Optics Express 12015, 2006. **14**: p. 69-81.

40.   Paschotta, R., *Fiber Amplifiers*, in *Encyclopedia of Laser Physics and Technology* 2008.

41.   Digonnet, M.J.F., *Rare Earth Doped Fiber Lasers and Amplifiers*. 1993, New York: Marcel Dekker, Inc.

42.   Paschotta, R., et al., *Ytterbium-Doped Fiber Amplifiers.* IEEE Journal of Quantum Electronics, 1997. **33**(7): p. 1049-1056.

43.   Pask, H.M., et al., *Ytterbium-doped silica fiber lasers: versatile sources for the1-1.2 μm region.* Selected Topics in IEEE Journal of Quantum Electronics, 1995. **1**(1): p. 2-13.

44.   Paschotta, R., Nilsson, Johan, Barber, P. R., Caplen, J.E., Tropper, Anne C., and Hanna, David C., *Lifetime quenching in Yb-doped fibers.* Optics Communications, 1997. **136**: p. 375-378.

45.   Leger, J.R., et al., *Coherent beam addition: An application of binary optics.* Lincoln Lab. J., 1988. **1**: p. 225-245.

46.   Fan, T.Y., *Laser beam combining for high-power, high-radiance sources.* IEEE J. of Selected Topics in Quantum Electron, 2005. **11**(3): p. 567-577.

47.   Fan, T.Y. and A. Sanchez, *Coherent (phased array) and wavelength (spectral) beam combining compared.* Proceedings of SPIE, 2005. **57209**: p. 157-164.

48.   Shay, T.M., et al., *First experimental demonstration of selfsynchronous phase locking of an optical array.* Optics Express, 2006. **14**(25): p. 12015-12020.

49.   August, S.J., T.Y. Fan, and A. Sanchez, *Coherent Beam Combining and Phase Noise Measurements of Yt fiber Amplifiers.* Optics Letters, 2004. **29**: p. 474-476.

50. Shay, T.M., et al., *Self-Synchronous and Self-Referenced Coherent Beam Combination for Large Optical Arrays.* IEEE J. of Selected Topics in Quantum Electron, 2007. **13**(3): p. 480-486.

51. IPG. *YLR-HP Series: 1-50kW Ytterbium Fiber Lasers* 2009 [cited 2009 March]; Available from: http://www.ipgphotonics.com/products_1micron_lasers_cw_ylr-hpseries.htm.

52. Ruffin, A.B., et al., *Brillouin gain analysis for fibers with different refractive indices.* Optics Letters, 2005. **30**: p. 3123-3125.

53. Kobyakov, A., et al., *Design concept for optical fibers with enhanced SBS threshold.* Optics Express, 2005. **13**: p. 5338-5346.

54. Ward, B.G., C. Robin, and M. Culpepper. *Photonic crystal fiber designs for power scaling of singlepolarization amplifiers.* in *Photonics West.* 2007. San Jose, CA.

55. Bronder, T.J., et al., *SBS mitigation with 'two-tone' amplification: a theoretical model.* Proc. of SPIE, 2008. **6873**

56. Dajani, I., et al., *A theoretical treatment of two approaches to SBS mitigation with two-tone amplification.* OPTICS EXPRESS 14233, 2008. **16**(18).

57. Russell, P., *Photonic Crystal Fibers*, in *Science Magazine*. 2003. p. 358-362.

58. Fabelinkii, I.L., *Molecular Scattering of Light.* 1968, New York: Plenum Press.

59. Stowe, K., *Introduction to Statistical Mechanics and Thermodynamics*. 1984, New York: John Wiley & Sons. 534.

60. Boyd, R.W. and K. Rzazewski, *Noise initiation of stimulated Brillouin scattering.* Physical Review A, 1990. **42**(9): p. 5514-5521.

61. Jeunhomme, L.B., *Single-mode fiber optics*. 1989, New York: Marcel Dekker, Inc.

62. Tang, C.L., *Saturation and spectral characteristics of the Stokes emission in the stimulated Brillouin process.* Journal of Applied Physics, 1966. **37**(8): p. 2945-2955.

63. Grower, P., *Optical Phase Conjugation*. 1994: Springer Verlag. 52-53.

64. Kovalev, V.I. and R.G. Harrison, *Suppression of stimulated Brillouin scattering in high-power single-frequency fiber amplifiers.* Optics Letters, 2006. **31**(2): p. 161-163.

65.   Brown, D.C. and H.J. Hoffman, *Thermal, Stress, and Thermo-Optic Effects in High Average Power Double-Clad Silica Fiber Lasers.* IEEE Journal of Quantum Electronics, 2001. **37**(2): p. 207-217.

66.   Mao, X.P., et al., *Stimulated Brillouin threshold dependence on fiber type and uniformity.* IEEE Photonics Technology Letters, 1992. **4**: p. 66-69.